Int J Fract (2015) 191:53–75
DOI 10.1007/s10704-015-9995-3

SPECIAL INVITED ARTICLE CELEBRATING IJF AT 50

Fracture in metallic glasses: mechanics and mechanisms

R. Narasimhan · Parag Tandaiya · I. Singh · R. L. Narayan · U. Ramamurty

Received: 3 December 2014 / Accepted: 24 January 2015 / Published online: 11 February 2015

Abstract Significant progress in understanding the mechanical behavior of metallic glasses (MGs) was made over the past decade, particularly on mechanisms of plastic deformation. However, recent research thrust has been on exploring the mechanics and physics of fracture. MGs can be very brittle with K_{Ic} values similar to silicate glasses and ceramics or very tough with K_{Ic} akin to high toughness crystalline metals. Even the tough MGs can become brittle with structural relaxation following annealing at temperatures close to glass transition temperature (T_g). Detailed experimental studies coupled with complementary numerical simulations of the recent past have provided insights on the micromechanisms of failure as well as nature of crack tip fields, and established the governing fracture criteria for ductile and brittle glasses. In this paper, the above advances are reviewed and outstanding issues in the context of fracture of amorphous alloys that need to be resolved are identified.

Keywords Metallic glasses · Crack tip fields · Vein patterns · Shear bands · Nanocorrugations · Cavitation

R. Narasimhan (✉) · I. Singh
Department of Mechanical Engineering, Indian Institute of Science, Bangalore 560012, India
e-mail: narasi@mecheng.iisc.ernet.in

P. Tandiaya
Department of Mechanical Engineering, Indian Institute of Technology-Bombay, Mumbai 400076, India

R. L. Narayan · U. Ramamurty
Department of Materials Engineering, Indian Institute of Science, Bangalore 560012, India

U. Ramamurty
Center of Excellence for Advanced Materials Research, King Abdulaziz University, Jeddah 21589, Saudi Arabia

1 Introduction

Mechanical behavior of metallic glasses (MGs) has been one of the most active areas of research in the structural materials arena over the past 15 years although they were first synthesized more than five decades back (Klement et al. 1960). Three major reasons can be attributed to this surge in the interest on MGs. First is the discovery of multi-component alloy compositions that do not crystallize even when cooled relatively slowly which enabled MGs to be produced in 'bulk' form. The second reason is the realization that these 'bulk metallic glasses (BMGs)' with their attractive combinations of mechanical properties (Schuh et al. 2007) are candidates as structural materials in a number of frontier areas of technology. However, understanding plastic deformation and fracture in these materials requires completely new thinking. This is because dislocation mechanics, which forms the basis for most of the theories on above topics in crystalline metals and alloys, cannot be invoked since MGs lack long range order. Consequently, there has been considerable scientific curiosity in unraveling the physics of deformation and fracture, which is the third

reason for the significant volume of research on the mechanical behavior of MGs.

The recent interest in MGs led to considerable progress in understanding their deformation response. By contrast, there is no such consensus on the fracture mechanisms and the mechanics of fracture. This is in spite of the fact that low fracture toughness and lack of crack growth resistance coupled with poor ductility are serious impediments for realizing the full potential of these new structural materials. The paucity of systematic fracture experiments on BMGs can be attributed to (a) the absence of a 'microstructure' in BMGs that would otherwise enable identification of the relevant material length scales and (b) extreme sensitivity of the measured toughness to the alloy composition, structural state, and other parameters many of which are difficult to monitor. Consequently, many researchers have interpreted the micromechanisms of fracture from fractographic observations, which has led to several contradictions. Nevertheless, some clarity due to combined experimental and computational studies has emerged in the recent past, which is summarized in this review. At this juncture, it is important to note that the sole emphasis of this review is to summarize mechanics-based approaches for understanding the fracture behavior of BMGs. The reader is referred to the review by Schuh et al. (2007) for a comprehensive overview of elastic and plastic deformations in BMGs and to a review by Xu et al. (2010) for a summary of the effect of composition and other structural aspects on the fracture toughness of BMGs.

2 Plastic deformation

Although the emphasis of the current paper is on fracture, some basic understanding of the mechanisms of plastic deformation that occur in amorphous alloys is essential. Hence, they are briefly discussed here (see Schuh et al. 2007; Greer and Ma 2007 for detailed reviews). While most MGs exhibit sufficient levels of plastic deformation, the underlying mechanisms are quite different from crystalline metals in which mobility of dislocations plays a vital role. Extensive computer simulations have firmly established that plastic flow units in MGs are shear transformation zones (STZs) proposed first by Argon (1979), which are clusters of atoms undergoing collective shear deformations under the influence of the applied stress (Falk 1999; Johnson and Samwer 2005; Zink et al. 2006). STZs occur preferably at locations where free volume, which is an intrinsic state parameter that embodies the atomic packing efficiency in the glass, is more. The activation of STZs is associated with considerable local dilatation, which makes the macroscopic plastic flow pressure sensitive (Lu and Ravichandran 2003; Patnaik et al. 2004). Above the glass transition temperature, T_g, of the alloy profuse activation of the STZs occurs and their stress field relaxes instantaneously, leading to homogenous flow of the glass (Schuh et al. 2007; Langer 2008). On the other hand, well below T_g, plastic deformation at higher stresses manifests in the form of shear bands (SBs), within which strain localization occurs. The atomic structure within the SBs shows increase in concentration of STZs and free volume (Sopu et al. 2009). Such localization of flow and concomitant flow softening during deformation, in conjunction with the fact that there are no intrinsic barriers such as grain boundaries to the SBs, results in near-zero ductility of MGs. In compression or in constrained deformation conditions such as indentation, it is possible to induce multiple shear banding (Lu and Ravichandran 2003; Patnaik et al. 2004).

3 Ductile and brittle BMGs

Before describing the mechanisms and mechanics of fracture, it is instructive to examine the range of K_{Ic} values exhibited by BMGs and on that basis broadly classify them as 'ductile' or 'brittle'. In the following, BMGs that exhibit SB mediated plastic flow are referred to as 'ductile,' as they exhibit high levels of K_{Ic}. However, two important points are to be noted. (1) In spite of the high K_{Ic} values, these BMGs hardly show any R-curve behavior owing to lack of microstructural features like grain boundaries which can offer resistance to crack growth. (2) Unlike in crystalline metals and alloys wherein a one-to-one correspondence between ductility and toughness can typically be observed, no such correlation exists in BMGs. In fact, one can obtain high K_{Ic} in a BMG which exhibits zero tensile ductility! For ductile BMGs, the measured K_{Ic} values are comparable to crystalline counterparts. For example, K_{Ic} of Vitreloy-1 or Vit-1, a Zr based BMG that is widely studied due to its commercial availability, is $\sim$55 MPa m$^{1/2}$ (Conner et al. 1997; Gilbert et al. 1997) whereas a Pt-based BMG developed by Schroers and Johnson (2004) has a K_{Ic} of about 80 MPa m$^{1/2}$.

In many BMGs however, SB mediated plasticity does not occur at all. Consequently, they exhibit low K_{Ic} values in the range of ~0.5–15 MPa $m^{1/2}$ (Pan et al. 2007; Wang et al. 2009; Narayan et al. 2014) and hence are termed as 'brittle'. While some BMGs such as Fe- and Mg-based ones are brittle in the as-processed condition itself, some tough BMGs can be made brittle through annealing at temperatures below T_g, a process referred to as structural relaxation (Duine et al. 1992; De Hey et al. 1998). Yet, some other glasses are also brittle, but only under specific combinations of experimental conditions (typically low temperatures and high strain rates) (Jiang et al. 2008; Hasan et al. 2008). Hasan et al. (2008) examined the effects of temperature and loading rate on fracture toughness and mechanism in Vit-1. They found that as temperature changes from $0.8T_g$ to T_g, there is a sharp increase in the fracture toughness with the behavior changing from plane strain (flat fracture) to plane stress (shear fracture). In general, increasing the strain rate caused decrease in the toughness, especially at high temperatures (above $0.9T_g$).

Alloy composition (Kawashima et al. 2005; Kim et al. 2009), as well as several extrinsic parameters like low cooling rate (Gu et al. 2009; Tan et al. 2011), structural relaxation (Murali and Ramamurty 2005; Raghavan et al. 2006; Kumar et al. 2009), partial crystallization (Nagendra et al. 2000), and presence of impurities (Conner et al. 1997; Lowhaphandu and Lewandowski 1998; Keryvin et al. 2006) are known to be responsible for this brittle behavior. Structural relaxation reduces the free volume (De Hey et al. 1998; Murali and Ramamurty 2005) and thereby limits the operation of localized atomic shear transformations, which in turn inhibits the formation of SBs. Since SBs contribute to plasticity in BMGs at low temperatures (well below T_g) and high stresses (Schuh et al. 2007), their absence results in brittleness.

4 Ductile fracture

4.1 Mechanism

A characteristic feature of fracture surface in ductile BMGs is the presence of "vein patterns", which are akin to those observed after separating two glass slides with a thin viscous medium in-between them (see, for example, Leamy et al. 1972; Pampillo 1975; Qu et al. 2010). The occurrence of these patterns can be attributed to reduction in viscosity during deformation within the shear bands and consequent instability in the fluid meniscus (Saffman and Taylor 1958; Argon and Salama 1976). Some recent observations by Tandaiya et al. (2013) on the mechanism of ductile fracture in BMGs are presented below.

A low magnification scanning electron micrograph obtained from the fracture surface of a ductile notched BMG specimen, which was tested in four point bending configuration, is shown in Fig. 1a. Three distinct morphologies adjacent to the original notch front (extreme-left white dashed line) can be seen from it. First, a smooth region around 12 μm in width, which corresponds to about half the notch opening displacement, adjacent to the notch front is noticed. This is due to blunting of the notch at the line of intersection of a dominant shear band with the notch root. Next is the Taylor or fluid meniscus instability (FMI) region, in which vein or ridge patterns that run nominally perpendicular to the notch front may be seen. A higher magnification image of the FMI region (Fig. 1b) shows a set of parallel veins emanating almost perpendicular to the notch front. The third zone, which starts from the end of FMI region, pertains to dynamic crack propagation and is characterized by coarse dimple-like patterns superimposed on ridges and valleys. The fracture process zone length, L_c involving the notch blunting and FMI regions is about 65 μm in length. Similar fractographic features were also reported by Suh et al. (2010) close to the fatigue pre-crack front in Zr-based BMGs.

The above fracture features are rationalized by recourse to Argon and Salama (1976)'s model, who postulated that the convex notch front behaves as a fluid meniscus which advances under the suction (or hydrostatic stress) gradient, $d\sigma_h/dx$, prevailing in front of the notch root. By considering a perturbation in the notch front in the specimen thickness direction with wavelength λ, they argued that the perturbation will grow unstably in the form of a parallel set of fingers if $d\sigma_h/dx$ exceeds that caused by surface tension. Thus, they arrived at a preliminary estimate for the critical wavelength as $\lambda_c = 2\pi\sqrt{\chi/(d\sigma_h/dx)}$, where χ is the surface tension. Next, by analyzing meniscus instability in channel flow, a more precise estimate for λ_c was obtained as $\sqrt{3}$ times the above value. Using this estimate along with the hydrostatic stress distribution ahead of the notch tip computed from elastic–plastic finite element analysis, Tandaiya et al. (2013) deter-

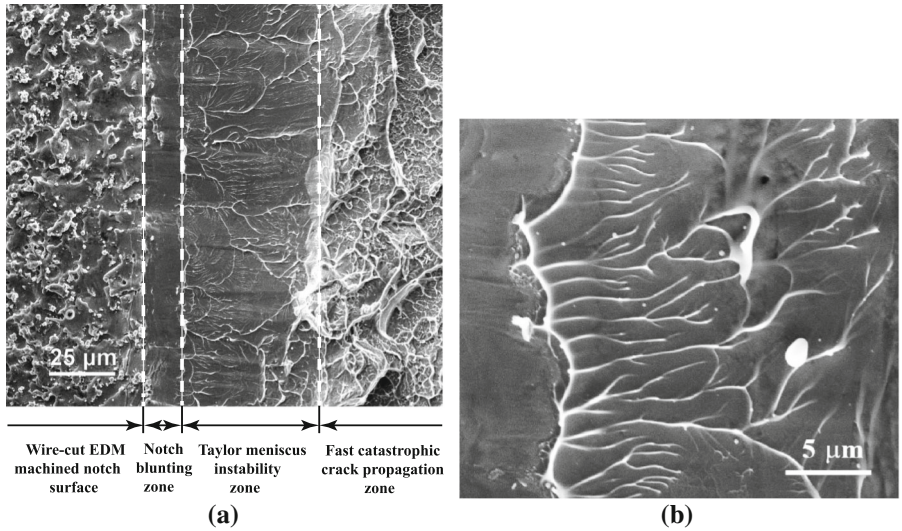

Fig. 1 **a** Low magnification scanning electron micrograph of fracture surface near a notch front in Vit-1 and **b** higher magnification image of the FMI region shown in **a**. Crack growth direction is from left to right in **a**, **b** (reprinted from Tandaiya et al. 2013 with permission from Elsevier)

mined λ_c as 1.76 μm which matches well with the mean ridge spacing measured from Fig. 1b.

Further, Argon and Salama (1976) considered the fingers as hollow circular cylinders of a nonlinear viscous solid with strain rate exponent $n(0 < n < 1)$ experiencing radial expansion. By equating the strain rate at the tip and root of the fingers from this analysis with that given by the notch root slip line field of Rice and Johnson (1970), the steady-state length of the fingers was determined. Finally, to relate to the channel flow analysis, the channel height was taken as crack tip opening displacement (δ). The expressions for the critical wavelength λ_c and CTOD δ_c thus obtained from their analysis are given by:

$$\lambda_c = 12\pi^2 A(n)\frac{\chi}{\tau_o}$$
$$\delta_c = 24\pi^2 B(n)\frac{\chi}{\tau_o} \quad (1)$$

Here, τ_o is shear yield strength and $A(n)$, $B(n)$ are parameters that depend on the rate exponent n. $A(n)$ increases from about 1.2–9, while $B(n)$ increases from around 1.5 to more than 100 as n changes from 0 (rate independent limit) to 0.5 (highly rate sensitive case).

Tandaiya et al. (2013) noted that crack grows within a dominant SB as can be seen from Fig. 2 for the mode I case. Here the crack propagates within the curved SB denoted by ABC and thereafter extends straight ahead of the notch tip. Similar crack growth in curved SBs had been observed earlier by Flores and Dauskardt (1999)

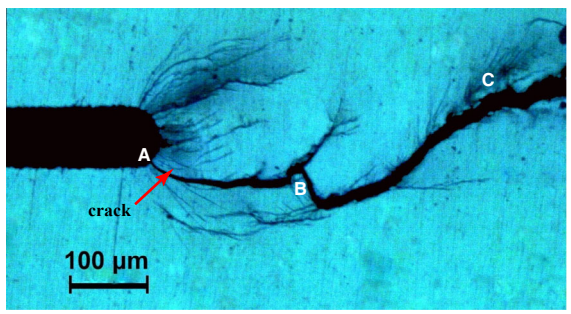

Fig. 2 Optical micrograph showing crack growing along a curved shear band ABC under mode I loading in an as-cast Vit-1 specimen (reprinted from Tandaiya et al. 2013 with permission from Elsevier)

for Vit-1. This contradicts the assumptions made in the Argon–Salama (A–S) model that the fingers develop ahead of the blunting crack tip and they grow as hollow circular cylinders experiencing radial expansion. Hence, Tandaiya et al. (2013) proposed a modified FMI model which is shown schematically in Fig. 3. Here, a dominant inclined SB first forms at the notch root (Fig. 3a) within which viscosity is reduced due to structural evolution and temperature rise. The convex notch surface acting as a fluid meniscus breaks down under the action of hydrostatic stress gradient prevailing ahead of the notch tip into a set of parallel, flattened fingers that penetrate the viscous fluid layer (Fig. 3b). Thus, the SB contains collinear elliptical cavities that grow under the action of normal stress σ_n and the ligaments connecting them eventually rupture (Fig. 3c, d) leading to crack growth within the SBs. This model

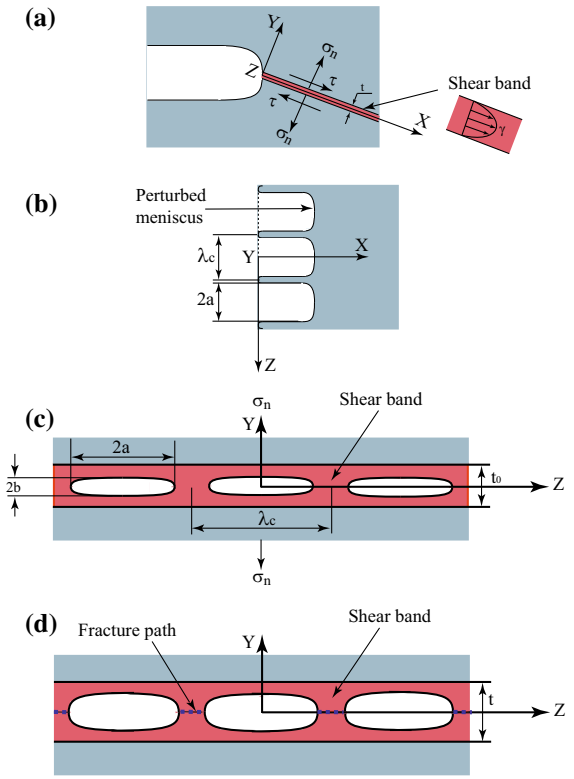

Fig. 3 Schematic of modified FMI model proposed by Tandaiya et al. (2013). **a** Dominant inclined shear band, **b** plan view showing perturbed meniscus, **c** edge view of shear band containing collinear elliptical cavities that correspond to the cross-sections of flattened cylindrical fingers and **d** growth of cavities under normal stress σ_n leading to rupture of ligaments connecting them (reprinted from Tandaiya et al. 2013 with permission from Elsevier)

suggests that the energy release rate J_c at crack initiation should scale with the ridge heights H which correspond to the critical opening displacements of the collinear cavities (see Fig. 3d). This was confirmed by Tandaiya et al. (2013). However, they did not find such a correlation between J_c and the spacing λ between the ridges or the fracture process zone length L_c. The latter was shown to correspond with the distance ahead of the tip over which $d\sigma_h/dx > 0$ at crack initiation.

4.2 Mechanics of crack tip fields and fracture criterion

In order to fully understand the fracture behavior of BMGs, it is necessary to characterize the stress and deformation fields present near a crack tip. Further, such an analysis can pinpoint the governing fracture criterion when combined with experimental observations. With this motivation, Tandaiya et al. (2007, 2009) studied stationary crack tip fields in BMGs under plane strain, small scale yielding conditions pertaining to mode I and mixed-mode loading using finite element simulations. This was complemented by experiments on Vit-1 (Tandaiya et al. 2009). The numerical simulations performed in the above studies made use of the Mohr–Coulomb based finite deformation constitutive model for BMGs proposed by Anand and Su (2005). This model incorporates several key features that are unique to plasticity in BMGs such as sensitivity of yielding to hydrostatic stress and normal as well as shear stress on the slip plane, shear induced dilatation and softening triggered by free volume evolution (Argon 1979; Spaepen 1977; Donovan 1989; Bhowmick et al. 2006; Lu and Ravichandran 2003; Patnaik et al. 2004; Lund and Schuh 2003).

In Fig. 4a, b, the angular distribution of normalized tangential stress $\sigma_{\theta\theta}/c_o$, where c_o is the initial value of cohesion, and maximum principal logarithmic plastic strain $\log(\lambda_1^p)$ around the notch tip for mode I are displayed at a normalized radial distance $r/(J/c_o) = 1.5$ from the notch tip for three different values of internal friction parameter μ. It can be observed from Fig. 4a that there is a dramatic decrease in $\sigma_{\theta\theta}$ at $\theta = 0°$ with increase in μ which diminishes with θ. Figure 4b shows that at angles $\theta \leq 90°$, the plastic strain level enhances strongly with increase in μ. Also, as μ increases, many serrations in the near-tip angular distribution of plastic strain can be observed, which suggests a tendency for plastic strains to localize into discrete shear bands, as observed in experiments (see Fig. 2).

Under mixed mode loading, an increase in the mode II component of loading was found to dramatically enhance the plastic zone size normalized by $(|K|/c_o)^2$, lower the stresses but significantly elevate the plastic strain levels near the notch tip (Tandaiya et al. 2009). Higher internal friction reduces the peak tangential stress but increases the plastic strain and stretching near the blunted part of the notch. In Fig. 5, the radial variation of $\sigma_{\theta\theta}/c_o$ for $\mu = 0.15$ is plotted for different remote elastic mode mixities $M_e = 2/\pi \tan^{-1}(K_I/K_{II})$. The stresses are extracted corresponding to angles at which $\sigma_{\theta\theta}/c_o$ is maximum at $r/(J/c_o) = 2$ for the respective mixed mode loading cases. It can be seen from the figure that the peak magnitude of $\sigma_{\theta\theta}$ is highest for $M_e = 1$ (pure mode I) and lowest for $M_e = 0$ (pure mode II).

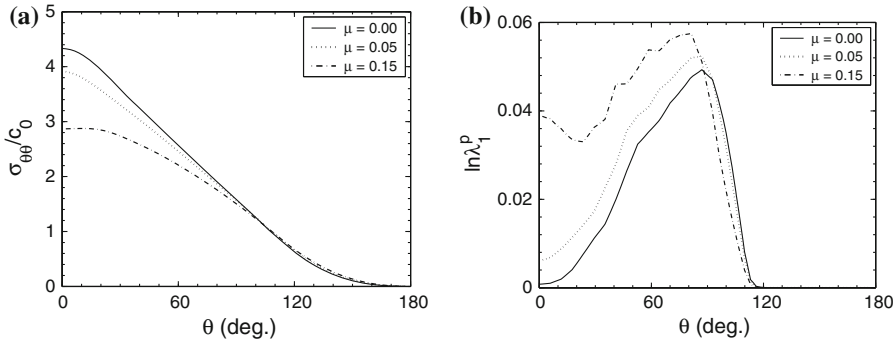

Fig. 4 Angular variation of **a** tangential stress normalized by initial value of cohesion c_o and, **b** maximum principal logarithmic plastic strain around the notch tip at normalized radius of $r/(J/c_o) = 1.5$ for different values of friction parameter (reprinted from Tandaiya et al. 2007 with permission from Elsevier)

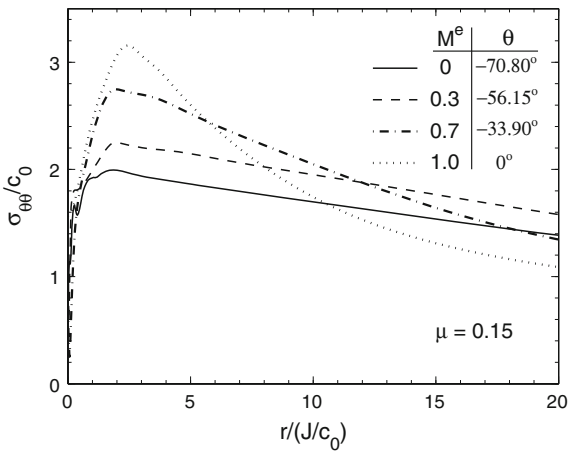

Fig. 5 Radial variation of normalized tangential stress showing the effect of mode mixity for $\mu = 0.15$ (reprinted from Tandaiya et al. 2009 with permission from Elsevier)

By statistically distributing the initial cohesion among the elements of the mesh, Tandaiya et al. (2007, 2009) simulated discrete shear bands near the notch tip. In Fig. 6, the shear band patterns near the notch tip predicted from finite element simulations are compared with those observed in the experiments for the pure mode II loading. The coordinate axes are normalized by the initial notch diameter b_o. Figure 6a displays contour plots of $\log(\lambda_1^p)$ showing the simulated shear bands near the notch root for $\mu = 0.05$ in the deformed configuration at $J/(c_o b_o) = 0.2$. In this figure, the lowest contour of $\log(\lambda_1^p) = 0.001$ gives a representation of the elastic–plastic boundary. Figure 6b shows the optical micrographs of the near-tip region at the same level of $J/(c_o b_o)$ as in Fig. 6a. In this figure, a dashed curve is drawn to roughly indicate the boundary of the shear banded region. It can be seen from Fig. 6a that the plastic zone predicted from finite element simulation consists of several straight SBs emanating from the notch (unlike mode I case) and is similar to the optical micrograph (Fig. 6b). Also, Fig. 6a shows that a dominant SB occurs at about $\theta \sim -10\circ$ with respect to the notch line and extends to a distance of $8b_o$ ahead of the notch tip which is in accord with the experiment. Indeed, crack growth occurs along this SB as observed in the experiments of Tandaiya et al. (2009, 2013) and also the mode II experiments of Flores and Dauskardt (2006) on a Zr-based BMG.

Tandaiya et al. (2009) employed a critical plastic strain criterion which postulates that crack initiation would take place when $\log(\lambda_1^p)$ at some angle θ with respect to the notch line exceeds a critical value ε_c over a critical radial distance (fracture process zone length) r_c^ε from the notch tip in order to predict the variation of notched fracture toughness J_c versus M_e. This criterion is appropriate for the as-cast Vit-1 tested by Tandaiya et al. (2009) since crack propagation occurred within a dominant SB in all mixed-mode cases following the modified FMI mechanism discussed in Sect. 4.1, which is expected to be strain-controlled. The examination of SEM fractograph of the fractured specimens (see, for example, Fig. 1a) leads to the identification of the fracture process zone length to be about 60 μm (which in this case is equal to $b_o = 2r_o$, where r_o is the initial notch root radius). In Fig. 7, variations of J_c/J_o versus M_e predicted from the simulation results corresponding to different ε_c and r_c^ε/r_o are plotted along with the experimental data for Vit-1. Here, a reference value J_o obtained for the case $M_e = 0$ by employing the fracture criterion with $\varepsilon_c = 0.1$ and $r_c^\varepsilon/r_o = 2$ is used for the purpose of normalization.

It can be seen from Fig. 7 that the critical strain criterion predicts a monotonically decreasing toughness from mode I to mode II, owing to strong increase in plastic strain at the same level of J as mentioned ear-

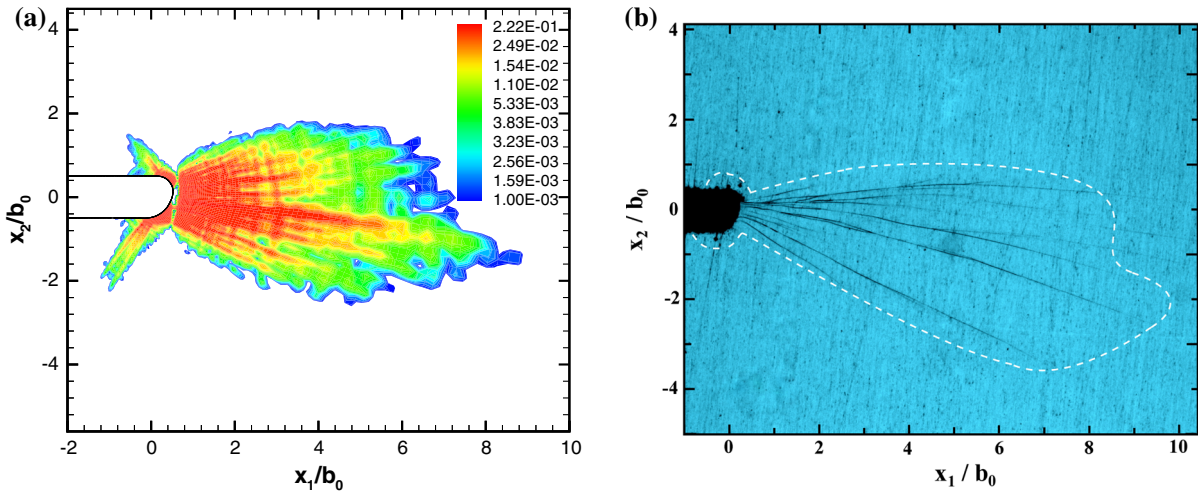

Fig. 6 Comparison of shear band patterns near the notch tip obtained from simulations and experiments for mode II loading ($M_e = 0$) at $J/(c_o b_o) = 0.2$. **a** Contour plots of maximum principal logarithmic plastic strain for $\mu = 0.05$ and **b** optical micrograph of the near-tip region obtained from experiments (reprinted from Tandaiya et al. 2009 with permission from Elsevier)

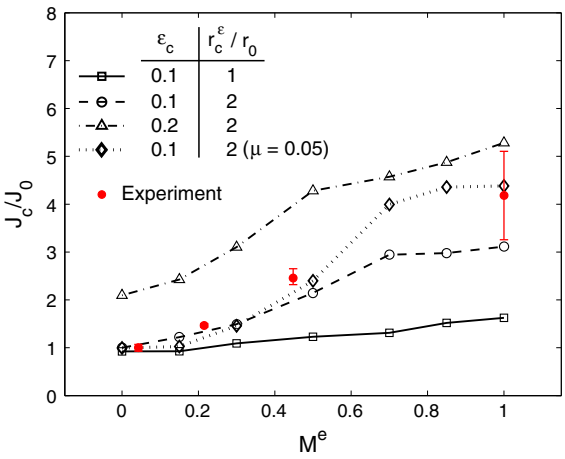

Fig. 7 Predicted variation of normalized fracture toughness with mode mixity for $\mu = 0.15$ assuming a strain controlled fracture criterion along with data obtained from mixed mode fracture experiments for as-cast Vit-1 (reprinted from Tandaiya et al. 2009 with permission from Elsevier)

lier (Tandaiya et al. 2009). The results shown in Fig. 7 suggest that if a ductile fracture mechanism is operative for all M_e cases, the predicted ratio of mode I to mode II toughness could range from 1.75 to 4. It can also be seen from Fig. 7 that the experimental data for the notched Vit-1 specimens validates the predicted J_c versus M_e variation for $\mu = 0.05$ and a process zone size $r_c^{\varepsilon}/r_o = 2$, which is identified from the fractographs and $\varepsilon_c = 0.1$. Another interesting observation is that the scatter reduces as $M_e \rightarrow 0$. Thus, the mixed-mode experimental data are highly repeatable as opposed to the pure mode I case. Tandaiya et al. (2009) also made predictions of J_c versus M_e based on a critical tangential stress criterion to mimic brittle fracture processes. They postulated that possible transitions from brittle to ductile mode of fracture may occur as M_e decreases from 1 (at some intermediate value of M_e). They also showed that different trends in J_c versus M_e are possible based on the operative fracture mechanism and level of critical stress and strain as well as the process zone lengths.

Varadarajan et al. (2010) reported from mixed-mode fracture experiments on Zr-based BMGs that the fracture energy increases as the loading changes from mode I. Further, nominal addition in mode II component ($M_e \sim 0.83$) showed strong kinking of the crack (see Figs. 2 and 11 of their paper). It is not clear if the fracture paths observed in their experiments were dictated by shear bands as in the experiments of Flores and Dauskardt (2006) and Tandaiya et al. (2009, 2013). The mode II fracture toughness K_{IIc} was measured by Flores and Dauskardt (2006) for Vit-1 as 75 MPa $m^{1/2}$, whereas their mode I tests (Flores and Dauskardt 1999) had indicated that $K_{Ic} \sim 130$ MPa $m^{1/2}$. However, the mode I stress intensity factors at the tips of branched cracks estimated by them were around 15 MPa $m^{1/2}$.

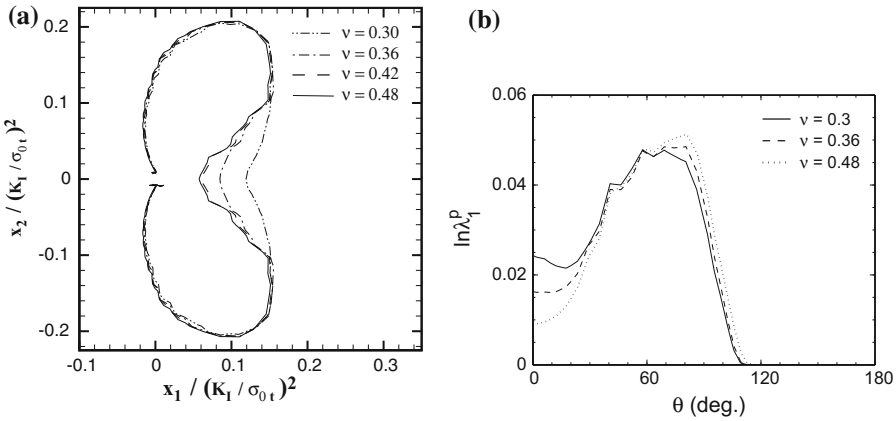

Fig. 8 Effect of Poisson's ratio on **a** the plastic zone (plotted in normalized coordinates) and **b** near-tip angular distribution of maximum principal logarithmic plastic strain at a normalized radial distance of $r/(J/\sigma_{ot}) = 3.3$ from the notch tip (reprinted from Tandaiya et al. 2008 with permission from Elsevier)

Schroers and Johnson (2004) suggested that the high K_{Ic} of a Pt-rich BMG is due to its large Poisson's ratio, $\nu = 0.42$ (or, equivalently low shear modulus, G, to bulk modulus, κ, ratio). It was suggested that a low G/κ ratio promotes shear deformation and inhibits crack opening due to dilational flow. Taking cue from this, Lewandowski et al. (2005) reported a correlation between fracture energy and ν of various MGs similar to that pointed out first by Pugh (1954) for polycrystalline metals. It was noted that MGs with higher ν tend to be tougher. The critical value of ν that demarcates brittle and ductile behavior is around 0.32. The observed strong correlation between toughness and ν in MGs is intriguing because they are isotropic and do not exhibit dislocation mediated plasticity (Rice and Thomson 1974). Further, ν is a parameter that captures the coupling of longitudinal and transverse elastic deformations, which are small in the context of metallic materials, whereas the fracture energy pertains to ultimate material failure and involves large deformations at least locally. If the Poisson's ratio coupling influences the development of plasticity, then this effect would depend significantly on specimen thickness and should still only influence the amount of plastic work, and not the fracture work. Nevertheless, the correlation postulated by Lewandowski et al. (2005) has led many researchers working in the field to pursue developing BMGs with high ν, while the micro-mechanical origins of this correlation are not clearly understood.

In order to gain a mechanics perspective, Tandaiya et al. (2008) conducted a parametric study of the effect of ν on the stationary mode I crack tip fields in metallic glasses using the BMG constitutive model mentioned earlier. In Fig. 8a, the plastic zones obtained from the finite element simulations corresponding to different ν (in the range from 0.3 to 0.48) are presented in normalized coordinates. It can be seen that increasing ν from 0.3 to 0.42 causes a dramatic reduction in the plastic zone extent ahead of the notch tip (by more than 50 %). Figure 8b presents the effect of ν on the near-tip angular distribution of $\log(\lambda_1^p)$. Again, a strong decrease in plastic strain with enhancement in ν can be perceived. Further, Tandaiya et al. (2008) simulated SB formation near the notch root (using statistical distributions of cohesion) and showed that the plastic strains within individual SBs also reduce with increase in ν. While this may retard crack propagation along SBs to some extent, if a strain controlled mechanism is operative and in turn enhance the fracture toughness, the analysis performed by Tandaiya et al. (2008) shows that the correlation reported by Lewandowski et al. (2005) lacks a strong mechanics based rationale.

5 Brittle fracture

5.1 Crack initiation

All brittle BMGs exhibit similar and distinct fracture features irrespective of the composition, thermal history or the testing conditions employed (see, for example, Wang et al. 2007, 2008; Narayan et al. 2014). Fractographs of brittle BMG specimens tested in mode I fracture configuration show the typical mirror, mist and hackle regions that are commonly observed in brittle ceramics and non-metallic glasses (Hull 1995, 1999). Thus, in the low resolution SEM image corresponding to embrittled Vit-1 (Narayan et al. 2014) shown in

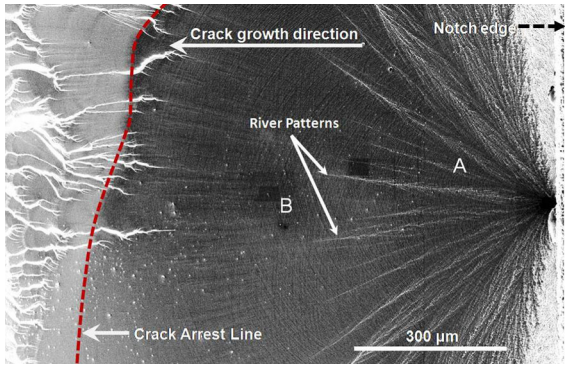

Fig. 9 Low magnification SEM image of the fracture surface from a pre-notched 4-point bending test of structurally relaxed Vit-1 showing macroscopic fracture features. '*A*' denotes the mist region and '*B*' is the mirror region (reprinted from Narayan et al. 2014 with permission from Elsevier)

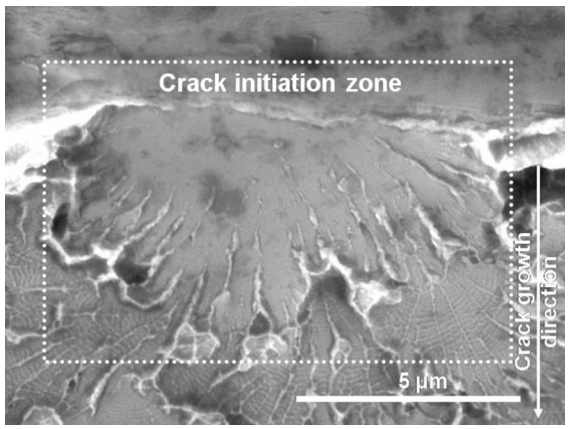

Fig. 10 HRSEM image of the featureless crack initiation zone near the notch front in annealed Vit-1 specimen. Small dimples/corrugations are visible beyond this semi-circular zone (reprinted from Narayan et al. 2014 with permission from Elsevier)

Fig. 9, the mist and mirror regions are labeled as A and B, respectively. The mist region A originates from the center of the notch edge forming a wide 'V-shaped' region surrounded by hackle. It also consists of river patterns that extend radially outward from the centre of the notch front.

Crack initiation occurs from the notch front at the mid-thickness of the specimen, which appears as a semi-circular featureless zone. This may be seen from Fig. 10 which is a high magnification image near the vertex of the V-shaped region marked as A in Fig. 9. It must be noted that the hydrostatic stress σ_h would be maximum ahead of the notch front at the mid-thickness owing to near-plane strain conditions caused by thickness constraint (Narasimhan and Rosakis 1990). Hence, Narayan et al. (2014) proposed that incipient cavitation occurs leading to the formation of the featureless half penny-shaped zone seen in Fig. 10. However, this is intriguing because the maximum σ_h attained in front of a blunting crack tip in an elastic–plastic solid is much lower than that required for a cavity to nucleate (Varias et al. 1991). For example, Huang et al. (1991) have shown that for a non-hardening solid with tensile yield strain of 0.003, the critical hydrostatic stress for cavitation is 4.3 times the tensile yield strength σ_o. By contrast, the maximum value of hydrostatic stress attained in front of a blunting tip in such a material is only about $2.4\sigma_o$ (McMeeking 1977).

Henann and Anand (2009) implicitly assumed that the cavitation strength scales with the bulk modulus of the material and also chose very low values for ratio of cavitation strength to yield strength (e.g., 0.8 for $\nu = 0.36$). With these assumptions, they showed that the fracture toughness correlates with ν and the square root of the notch root radius in BMGs as observed in the experiments of Lewandowski et al. (2006). It is however not clear why the cavitation strength should scale with the bulk modulus and also why the value of cavitation stress chosen is so low in comparison to that of elastic–plastic models as mentioned above (Huang et al. 1991).

Some important insights on the above discrepancy were obtained from the work of Murali et al. (2011) who conducted molecular dynamics simulations on a brittle FeP glass, and concluded that a cavitation mechanism is possible since critical hydrostatic stress at cavitation to yield strength ratio is only around 1.4. Murali et al. (2011) traced the origin of this behavior to the presence of strong nanoscale atomic density fluctuations in FeP glass with cavities always nucleating in regions of low density (or reduced yield strength). Motivated by this observation, Singh et al. (2013) conducted continuum analysis of cavitation in heterogeneous plastic solids with distributed weak zones and showed that cavitation stress is significantly reduced in relation to the yield strength (see Sect. 6). Thus, while crack initiation in ductile BMGs is controlled by a critical strain criterion as discussed in Sect. 4.2, a critical (hydrostatic) stress needs to be exceeded for crack initiation in brittle BMGs. Further evidence for this assertion is provided by the simulations results of

Rycroft and Bouchbinder (2012). Using a low temperature STZ model and Eulerian level set formulations to solve complex free boundary problems in a model BMG, they observed that with an increasing degree of embrittlement, crack initiation occurs at some distance ahead of the crack tip where σ_h reaches a maximum.

5.2 Crack propagation

Once the crack initiates in the brittle MG, it propagates dynamically as there are no microstructural features in the material to hinder its growth. The formation of river patterns seen in the mist region A in Fig. 9 has been attributed to the twisting of the crack front in the presence of local heterogeneities (Hull 1995; Narayan et al. 2014). To accommodate this twisting, the crack front breaks up into several segments. Each segment thereafter propagates at different levels and is separated by ridges that appear as river patterns on the fracture surface (Sommer 1969; Hull 1999). While the mirror region (marked as B in Fig. 9) appears macroscopically smooth, shiny and featureless, higher magnification imaging reveals the presence of highly regular and parallel nano-corrugations (NCs) perpendicular to the crack propagation direction (see Fig. 11). From atomic force microscope (AFM) section profiles taken along the crack propagation direction, Narayan et al. (2014) showed that NCs exhibit a distinct periodicity in their spacing. In the dynamic crack growth regime of brittle BMGs, NCs are the most ubiquitous features on the fracture surface and Table 1 lists the reported peak to peak separation s between successive NCs. As can be seen, s ranges from ∼30 to 150 nm for different BMGs and sometimes within the same specimen (Shen et al. 2006; Wang et al. 2006, 2007; Pan et al. 2007; Zhao et al. 2009; Jiang et al. 2011). Specifically, $s \sim 70$ nm in the case of annealed Vit-1 tested by Narayan et al. (2014).

On the basis of Wallner lines (Hull 1996; Rabinovitch et al. 2006; Ravi-Chandar 2004) observed on the fracture surfaces, Narayan et al. (2014) deduced that the maximum velocity with which the crack propagates, V_c, is about 780 m/s (i.e., $0.33V_s$ or $0.35V_R$, where V_s and V_R are shear and Rayleigh wave speeds in the material). This, in turn, was utilized to infer the timescale of formation of NCs to be about 10^{-10}s. Further, using the expression given by Rice and Levy (1969) for the temperature rise ahead of the growing crack tip, along with the above V_c value, Narayan et al. (2014) estimated that the temperature near the tip may attain values close to T_g, which can lead to pronounced softening. These inferences were utilized to discuss possible mechanisms of crack growth in brittle BMGs, a topic that has been intensely debated in the literature.

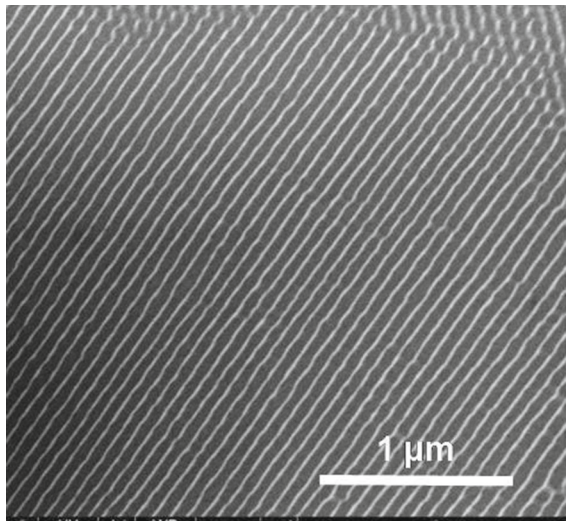

Fig. 11 SEM image in mirror region showing nano-corrugations or NCs in annealed Vit-1 specimen (reprinted from Narayan et al. 2014 with permission from Elsevier)

Many brittle materials exhibit wavy crack growth and micro-branching when the crack propagates above a critical velocity (Gao 1993; Ravi-Chandar and Yang 1997; Sharon et al. 2002; Ravi-Chandar 2004). Gao (1993) concluded on the basis of a perturbation analysis that at high speeds cracks tend to propagate along a wavy crack path so that the apparent crack velocity can be maintained at $0.5V_R$. Since the maximum crack velocity measured by Narayan et al. (2014) is only about $0.35V_R$, macroscopic instability in the dynamic crack front is unlikely. Also, unlike in silicate glasses, wherein wavy crack growth with perfect matching of the two fracture surfaces has been observed (Guin and Widerhorn 2004), fracture surfaces in brittle BMGs have been shown to exhibit peak-to-peak matching (Wang et al. 2007).

Since $T_{max} \sim T_g$, several authors (Pan et al. 2007; Wang et al. 2007, 2008, 2009; Jiang et al. 2008, 2010; Zhao et al. 2009) postulated that the formation of NCs is due to the FMI mechanism (see Sect. 4.1). A schematic of the FMI mechanism in brittle BMGs as suggested by Wang et al. (2008) is shown in Fig. 12. Since the material ahead of the crack tip is liquid-like at temper-

Table 1 Characteristic spacings of nano-corrugations (NCs) observed in different MGs

MG Composition	Specimen/loading conditions	NC spacing, s (nm)	References
$Zr_{41.2}Ti_{13.8}Cu_{10}Ni_{12.5}Be_{22.5}$	As-cast/high velocity impact	80	Jiang et al. (2008)
$Zr_{41.2}Ti_{13.8}Cu_{12.5}Ni_{10}Be_{22.5}$	Annealed/bending	71–80	Narayan et al. (2014)
$Zr_{55}Al_{22.5}Co_{22.5}$	As-cast/tension	83	Xia and Wang (2012)
$(Zr_{50.7}Cu_{28}Ni_9Al_{12.3})_{99}Gd_1$	As-cast/compression	74	Yajuan et al. (2009)
$Cu_{46}Zr_{42}A_{17}Y_5$	As-cast/bending	79	Xia and Wang (2012)
$Cu_{49}Hf_{42}Al_9$	As-cast/compression	74	Madge et al. (2009)
$Ni_{42}Cu_5Ti_{20}Zr_{21.5}Al_8Si_{3.5}$	As-cast/compression	60	Shen et al. (2006)
$Fe_{56}Mn_5Cr_7Mo_{12}Er_2C_{12}B_6$	As-cast/bending	36	Xia and Wang (2012)
$Fe_{65.5}Cr_4Mo_4Ga_4P_{12}C_5B_{5.5}$	As-cast/compression	15–52	Zhang et al. (2006)
$Fe_{66.7}Cr_{2.3}Mo_{4.5}P_{8.7}C_7B_{5.5}Si_{3.3}Al_2$	As-cast/compression	43	Li et al. (2007)
$Fe_{48}Cr_{15}Mo_{14}Er_2C_{15}B_6$	As-cast/compression	30	Ma et al. (2008)
$Fe_{73.5}Cu_1Nb_3Si_{13.5}B_9$	As-cast/tension	60	Wang et al. (2007)
$Fe_{78}Si_9B_{13}$	As-cast/tension	150	Kai-feng et al. (2007)
$Mg_{65}Cu_{20}Ni_5Gd_{10}$	As-cast/bending	50	Wang et al. (2007)
$Mg_{65}Cu_{25}Gd_{10}$	As-cast/bending	67	Pan et al. (2007)
$Mg_{65}Cu_{25}Tb_{10}$	As-cast/bending	83	Xia and Wang (2012)
$Tb_{36}Y_{20}Al_{24}Co_{20}$	As-cast/bending	90	Xia and Wang (2012)
$La_{62}Al_{14}Cu_{11.7}Ag_{2.3}Ni_5Co_5$	As-cast/bending	147	Xia and Wang (2012)
$La_{55}Al_{25}Ni_{10}Cu_5Co_5$	Annealed/charpy impact	120	Nagendra et al. (2000)
$Co_{43}Fe_{20}Ta_{5.5}B_{31.5}$	As-cast/compression	15–50	Zhang et al. (2006)
$Dy_{40}Y_{16}Al_{24}Co_{20}$	As-cast/bending	65	Wang et al. (2007)
$Pd_{40}Ni_{40}Si_4P_{16}$	As-cast/compression	50–200	Chen et al. (2009)

atures close to T_g, the crack tip is expected to act as a meniscus. When an infinitesimal perturbation of this meniscus reaches a critical wavelength (see Sect. 4.1), it grows and advances the crack front into the material. The plastic boundary within which the meniscus can grow is defined by the crack tip opening displacement (CTOD). When the meniscus finally extends till this boundary, a new blunt crack tip is produced along with a fluid zone ahead of it. The repetition of this process eventually results in the formation of NCs with a length scale corresponding to that of the CTOD.

Figure 13 highlights how an equiaxed dimpled structure formed near the crack tip evolves into a more continuous pattern (Xia and Wang 2012). A clear reduction in the waviness of the corrugations along their lengths with increasing distance from the crack tip can also be noted. To justify this reduction in the waviness, Xia and Wang (2012) suggested that FMI as well as stress-driven cavitation are competing crack growth mechanisms. However, it must be realized that the FMI model proposed by Argon and Salama (1976) predicts the formation of ridges/fingers that emanate *perpendicular* to the crack front (see Sect. 4.1; Fig. 1). Thus, the application of FMI mechanism to explain NCs that run *parallel* to the crack front might be inappropriate. Also, operation of FMI requires a positive hydrostatic stress gradient $d\sigma_h/dx$, whereas all studies that advocate this mechanism for brittle BMGs (Pan et al. 2007; Wang et al. 2007, 2008; Xia and Wang 2012) employ the stress field ahead of a sharp crack wherein this gradient is negative. Ignoring this fact, these studies use the absolute value of $\mathrm{d}\sigma_h/d\mathrm{x}$.

Dynamic cavitation ahead of the growing crack is another widely suggested mechanism for NC formation (Xi et al. 2005, 2006; Jiang et al. 2008, 2011). As will be discussed in Sect. 6, Singh et al. (2013, 2014a) have studied the mechanics of cavitation in brittle BMGs by taking into account fluctuation in strength. They have shown that for such a heterogeneous plastic solid, snap cavitation (i.e., sudden appearance of a void of finite size) is possible (see Sect. 6). A schematic of the probable cavitation mechanism is shown in Fig. 14. As can be

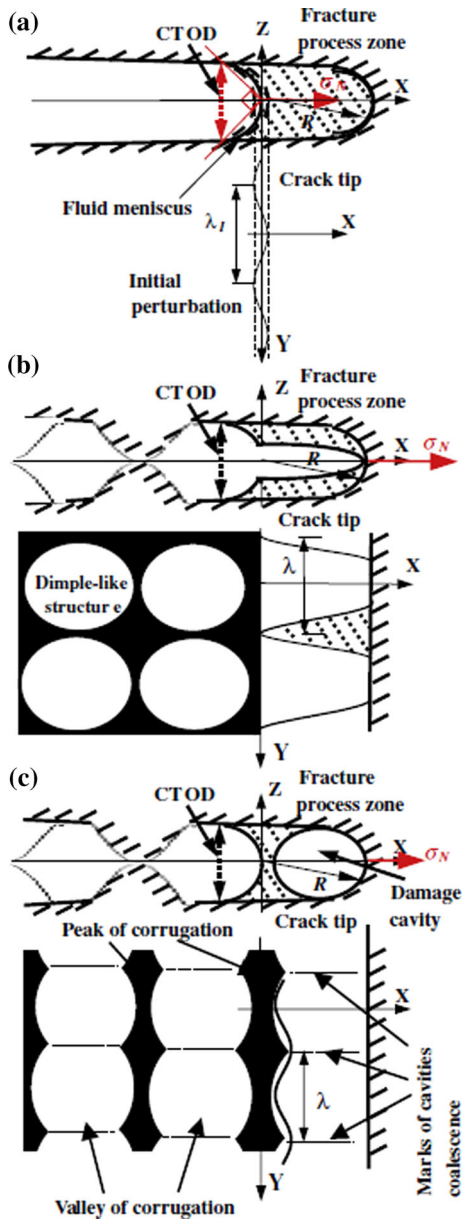

Fig. 12 Schematic of the crack propagation process assisted by the FMI mechanism. **a** Crack tip acting as the meniscus experiencing perturbations. **b** Growth of the perturbation under the hydrostatic stress gradient. **c** In-plane coalescence of voids leading to formation of NCs (reprinted from Wang et al. 2008 with permission from Elsevier)

seen from this illustration, repeated cavity nucleation in the softened region ahead of the crack tip followed by coalescence with it leads to the generation of a uniform NC pattern (Narayan et al. 2014).

Experimental observations of Wang et al. (2007) who showed peak-to-peak matching of the NCs across the two fracture surfaces and atomistic simulation results of Murali et al. (2011) support such a sequential cavitation–coalescence process. However, there are some issues that need to be resolved through further studies. First, the time scales of operation of STZs and atomic diffusion are much larger than that associated with formation of NCs. Thus, the fundamental plasticity mechanism behind dynamic cavitation needs to be addressed. Further, one expects the stochastic nature of atomic structure in BMGs to be reflected in the wavelength s of the NCs, whereas they are found to be highly periodic (Narayan et al. 2014). Singh et al. (2013) argue that the dominant wavelength in the strength fluctuations noted by Murali et al. (2011) may dictate the value of s. However, intriguingly, periodicity is not observed along the corrugations (Narayan et al. 2014).

6 Continuum analysis of cavitation in brittle metallic glasses

It is evident from Sect. 5 that a possible fracture mechanism in brittle BMGs is cavitation ahead of a crack tip. Also, as mentioned earlier, the results of Murali et al. (2011) have shown that the origin of cavitation in a brittle FeP glass is the presence of nanoscale fluctuations in atomic density giving rise to regions of reduced strength. Such nanoscale strength fluctuations in BMGs have been reported from nanoindentation experiments (Packard et al. 2010). This has provided motivation for examining the cavitation behavior of heterogeneous plastic solids with distributed weak zones (Singh et al. 2013, 2014a).

Several continuum studies of cavitation have been conducted in the context of homogeneous nonlinear elastic solids (Horgan and Abeyaratne 1986; Horgan and Pence 1989) and elastic–plastic solids (Huang et al. 1991; Hou and Abeyaratne 1992) using mean field theory. Horgan and Abeyaratne (1986) first demonstrated that the phenomenon of internal rupture is equivalent to the sudden rapid expansion of an infinitesimal void in a finite size body. Huang et al. (1991) and Hou and Abeyaratne (1992) noted that cavitation can be characterized in terms of attainment of a critical value of the hydrostatic stress if the remotely applied stress state is below yield. On the other hand, if the applied stress state is yielded prior to cavitation, then this critical stress may be significantly lower.

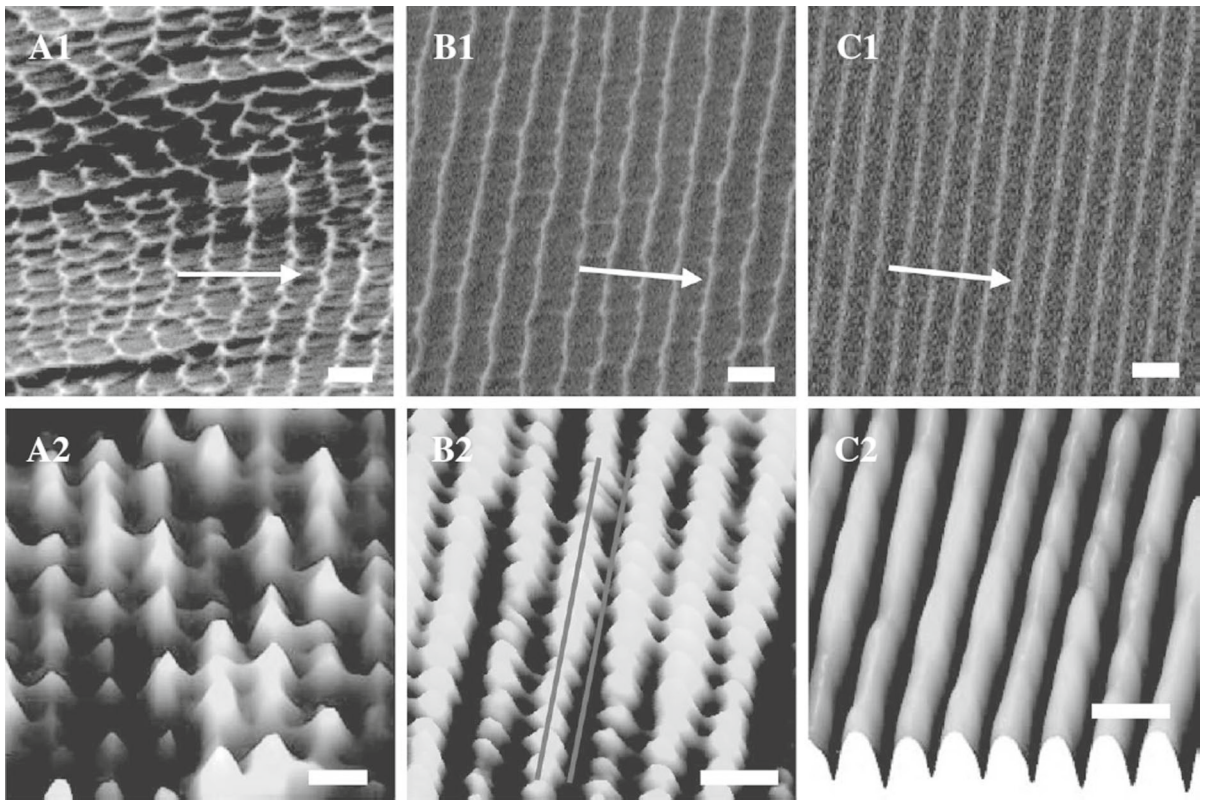

Fig. 13 **a–c** Evolution of the nanoscale features along the crack path (marked by *arrows*). Sequential SEM and AFM images show the transitioning of dimples into more continuous and parallel periodic stripes. Note that undulations along NCs vanish away from the crack tip in C2 (reprinted from Xia and Wang 2012 with permission from John Wiley and Sons)

6.1 Cavitation in heterogeneous elastic–plastic solids under equibiaxial stretching

Singh et al. (2013) modeled brittle BMGs as heterogeneous elastic–plastic solids containing a doubly periodic distribution of weak zones with yield strength, σ_{ow} lower than the strength σ_o of the background material. Finite element simulations of such solids were conducted by subjecting a square unit cell containing a circular weak zone at its center to equibiaxial stretching under plane strain conditions. A tiny void (with a very small volume fraction f_o) was placed at the center of the weak zone. The sudden rapid expansion of this void signifies cavitation (Hou and Abeyaratne 1992) and the corresponding macroscopic hydrostatic stress in the heterogeneous aggregate[1] Σ_{ha} is called as the cavitation stress Σ_c. Both the weak zone and background material were assumed to follow J_2 flow theory of plasticity with very low strain hardening. The values of σ_{ow}/σ_o and volume fraction f_{ow} of the weak zone were systematically varied to study their effect on cavitation behavior.

It was observed that in the presence of weak zones, a void nucleates in them at a hydrostatic level which can be considerably lower than that in a homogeneous plastic solid with no weak zones. Also, cavitation may occur before hydrostatic stress in the heterogeneous aggregate attains a peak at a value which is always close to that pertaining to the weak zone. Thus, the cavitation stress Σ_c is governed by the local properties of the weak zone, but does not depend on its volume fraction. This is clearly illustrated in Fig. 15 which shows a 3D plot of normalized cavitation stress Σ_c/σ_o as a function of yield strength ratio σ_{ow}/σ_o and f_{ow}. Also the simulations revealed

[1] Here, $\boldsymbol{\Sigma}$ and $\boldsymbol{\sigma}$ represent macroscopic stress in the aggregate and microscopic stress, respectively.

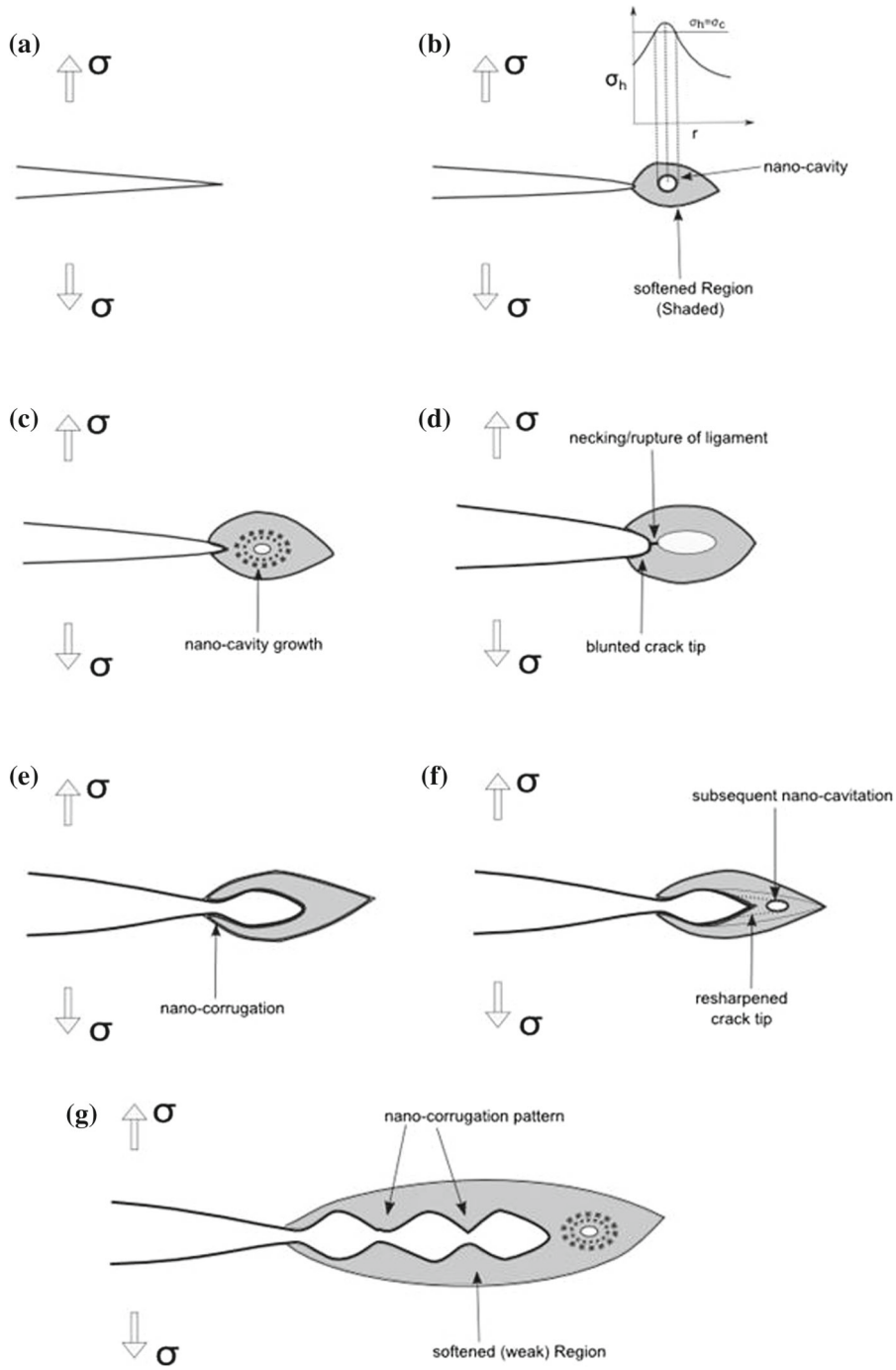

Fig. 14 Schematic of the cavitation mechanism: **a–c** remote loading on a sharp crack causing nanovoid nucleation by cavitation followed by growth and crack tip blunting; **d–e** rupture of ligament between the nanovoid and crack tip forming a nanocorrugation; **f** blunting of resharpened crack tip; **g** repeated operation of above processes leading to generation of NC patterns (reprinted from Narayan et al. 2014 with permission from Elsevier)

that even in the presence of a pre-existing void, a cavity nucleated in the weak zone will grow much faster than the former. These findings corroborate with the observations of Murali et al. (2011) pertaining to FeP glass.

Further, Singh et al. (2013) obtained analytical solutions for sudden expansion of an infinitesimal cylindrical void at the center of a composite cylinder with weak inner core and subjected to uniform radial traction under plane strain conditions. They reported differ-

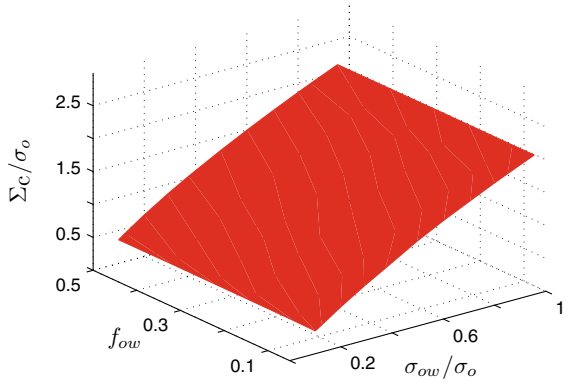

Fig. 15 Surface plot of normalized cavitation stress Σ_c/σ_o versus volume fraction f_{ow} and normalized yield strength σ_{ow}/σ_o of the weak zone (reprinted from Singh et al. 2013 with permission from Elsevier)

ent types of cavitation bifurcation patterns depending on the values of f_{ow} and σ_{ow}/σ_o of the core material. Figure 16a displays the variation of current volume fraction f of the infinitesimal void with respect to normalized macroscopic hydrostatic stress Σ_{ha}/σ_o in the composite cylinder for $\sigma_{ow}/\sigma_o = 0.2$ and $f_{ow} = 0.3$. Here, point 'c' refers to the onset of cavitation and Σ_{ha} associated with it is the cavitation stress Σ_c in the heterogeneous solid. Also, 'p' and 'q' are turning points where the nature of void growth may change from stable to unstable or vice versa. It can be seen from Fig. 16a that a finite sized void with volume fraction $f_{c\prime}$ would abruptly form when Σ_{ha} increases to $\Sigma_{c\prime}$ such that $\Sigma_q < \Sigma_{c\prime} < \Sigma_c$, where $\Sigma_{c\prime}$ and Σ_q are macroscopic hydrostatic stresses associated with the points 'c'' and 'q', respectively. It would expand stably till Σ_{ha} reaches Σ_p beyond which its growth becomes unstable. This situation is referred to as snap cavitation followed by smooth expansion of the void. Snap cavitation has also been predicted in composite nonlinear elastic spheres (see, for example, Horgan and Pence 1989). By contrast, Fig. 16b shows that for a large value of $f_{ow} = 0.9$, no snap cavitation occurs and the infinitesimal void expands unstably immediately after it nucleates.

6.2 Effect of stress state on cavitation response of heterogeneous plastic solids

Singh et al. (2014a) examined the effect of stress state on cavitation behavior of heterogeneous elastic–plastic solids. The finite element model and material properties used in this work are similar to Singh et al. (2013) except that the unit cell is subjected to biaxial stretching corresponding to different stress ratios $\rho = \Sigma_1/\Sigma_2$, where Σ_1 and Σ_2 are macroscopic stresses along X_1 and X_2 directions, respectively. For example, the ρ value prevailing ahead of a crack tip in a low hardening elastic–plastic solid is around 0.65. In order to characterize the stress state prevailing in the weak zone, a dimensionless parameter, $\omega_w = \bar{\sigma}_{ew}/\Sigma_{hw}$, where $\bar{\sigma}_{ew}$ and Σ_{hw} are the volume average of the von Mises equivalent stress and macroscopic hydrostatic stress in the weak zone, respectively, was introduced.[2] Singh et al. (2014a) observed substantial plastic yielding in the form of a shear band in the weak zone before onset of cavitation for low values of ρ, whereas it was insignificant corresponding to high ρ. Also, Σ_{hw} attains its peak value at onset of cavitation and drops rapidly thereafter.

Figure 17a plots variations of Σ_c/σ_o with ρ for different σ_{ow}/σ_o but with a fixed $f_{ow} = 0.1$. This figure shows that unlike in a homogeneous plastic solid (Huang et al. 1991; Hou and Abeyaratne 1992), only a marginal drop in Σ_c with reduction in ρ from 1 occurs for heterogeneous plastic solids when σ_{ow}/σ_o is low, whereas it becomes more pronounced with increase in σ_{ow}/σ_o. The above behavior can be rationalized by examining the variation of the critical value of stress state parameter ω_{wc} (value of ω_w at cavitation) with ρ for different values of σ_{ow}/σ_o shown in Fig. 17b. It can be observed that ω_{wc} increases marginally as ρ drops from 1 for low value of σ_{ow}/σ_o, whereas it enhances strongly for the same change in ρ for higher σ_{ow}/σ_o. Thus, in a heterogeneous plastic solid with low σ_{ow}/σ_o, the cavitation stress does not reduce much when ρ drops from 1 owing to marginal enhancement in ω_{wc} with reduction in ρ.

Singh et al. (2014a) also reported negligible effect of volume fraction of weak zone on the relationship between Σ_c and ρ as well as ω_{wc} and ρ. Figure 17c shows the variation of normalized cavitation stress Σ_c/σ_o for heterogeneous material (solid line curves) and cavitation stress Σ_{cw}/σ_o in a homogeneous material having the same properties as the weak zones (dashed line curves) with ω_{wc} for different values of σ_{ow}/σ_o. This figure pertains to $f_{ow} = 0.1$. It can be

[2] Note $\bar{\sigma}_{ew}$ is not equal to the Mises equivalent stress obtained from the macroscopic stress components.

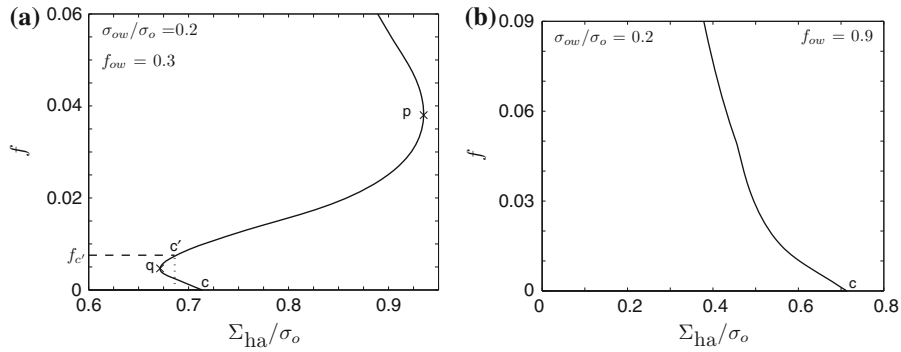

Fig. 16 **a** Variations of current volume fraction f of pre-existing infinitesimal void with normalized macroscopic hydrostatic stress Σ_{ha}/σ_o for an incompressible elastic–plastic composite cylinder pertaining to $\sigma_{ow}/\sigma_o = 0.2$ for **a** $f_{ow} = 0.3$ and **b** $f_{ow} = 0.9$ (reprinted from Singh et al. 2013 with permission from Elsevier)

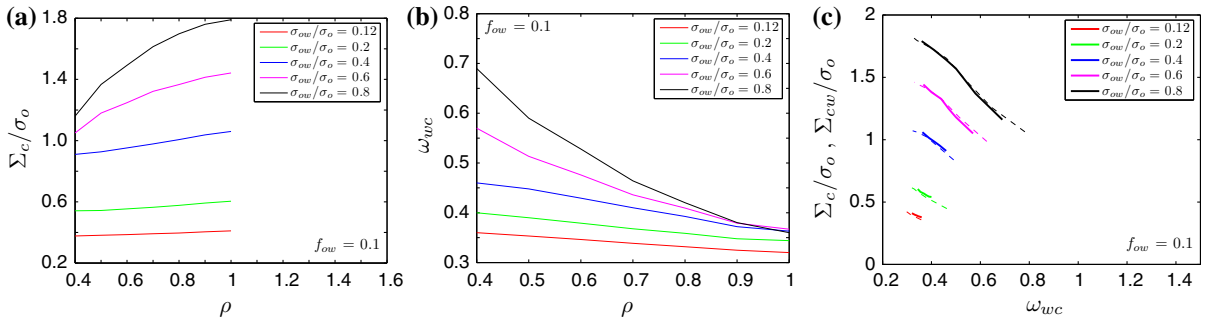

Fig. 17 Variations of **a** normalized cavitation stress Σ_c/σ_o with biaxiality ratio ρ and **b** critical value of stress state parameter ω_{wc} with ρ for $f_{ow} = 0.1$. **c** Variations of normalized cavitation stress Σ_c/σ_o in heterogeneous material (*solid lines*) and Σ_{cw}/σ_o in a homogeneous plastic solid (*dashed lines*) having the same properties as the weak zone (reprinted from Singh et al. 2014a with permission from Elsevier)

seen that Σ_c/σ_o drops with increase in ω_{wc} for all values of σ_{ow}/σ_o. Also, since ω_{wc} varies over a narrow range only a marginal drop in Σ_c/σ_o is noticed for small values of σ_{ow}/σ_o. Further, Σ_c/σ_o and Σ_{cw}/σ_o are close to each other which establishes that cavitation stress in a heterogeneous plastic solid is governed by yield properties and stress state prevailing in the weak zone as characterized by ω_w. Further, Singh et al. (2014a) showed that snap cavitation followed by stable growth of the void may take place for sufficiently high ρ, which transitions to smooth bifurcation at intermediate ρ and finally to unstable bifurcation to the left for sufficiently low ρ.

The above continuum studies have established that presence of weak zones in brittle BMGs will lower the cavitation stress, thereby making cavitation a plausible fracture mechanism in these materials as reported in atomistic simulations and experiments.

7 Size effects on tensile deformation and notch sensitivity in MGs

BMGs are considered quasi-brittle due to their negligible tensile ductility (Guo et al. 2007). Consequently, methods of improving ductility by engineering the BMG architecture (composites, nanoglasses, etc.) are being widely researched (see Sect. 8). An alternate avenue is to reduce the sample or feature size to nanoscale dimensions (Magagnosc et al. 2013). In-situ tension experiments conducted in electron microscopes on nanometer size MG samples (Guo et al. 2007; Jang and Greer 2010; Tian et al. 2012; Chen et al. 2013a; Magagnosc et al. 2013) have shown that transition in deformation behavior of MGs from quasi-brittle to ductile occurs when sample size is reduced below a critical value, which is of the order of 100 nm. Guo et al. (2007) reported around 23–45 % tensile ductility

including extensive necking or stable SB propagation in Zr-based MG. Necking was also observed in the experiments of Jang and Greer (2010) and Magagnosc et al. (2013) in focussed ion beam (FIB) milled MG specimens. While Jang and Greer (2010) noted that final failure happened by shear banding, Magagnosc et al. (2013) reported that the specimens failed by necking to a point. An important observation made by Guo et al. (2007) is that surface undulations in the form of shallow notches are present in 100 nm size samples and necking happens at these locations.

Further, these specimens show much higher strength compared to bulk samples and they display work hardening (Jang and Greer 2010; Tian et al. 2012; Chen et al. 2013a). The mechanistic reasons for the above behavior are not well understood although it is postulated that (a) the critical size required for an embryonic SB to grow unstably is not attained in nanometer size samples and (b) the stored elastic energy is not sufficient to drive the unstable growth of a SB as the specimen size is reduced to nanometer scale. This is because the elastic energy scales with the volume of the sample, whereas the energy required to create a SB scales with the cross-sectional area (like surface energy in the case of Griffith hypothesis).

An alternate viewpoint based on continuum analysis was put forward by Thamburaja (2011). He conducted finite element simulations using a non-local BMG constitutive model that accounts for free volume creation by plastic shearing as well as hydrostatic stress, diffusion and annihilation due to structural relaxation. Moreover, it has an in-built material length scale l_c associated with the interaction stress between flow defects such as STZs which controls the SB width (Thamburaja 2011). He showed that this interaction stress makes the deformation homogeneous when the specimen size is reduced, whereas the larger specimens fail by unstable growth of a shear band.

Molecular dynamics simulations on nanoscale MG samples with pre-existing notches show that local yielding at notch root relaxes the stress concentration and makes normalized tensile strength insensitive to the presence of the notch, while shear band nucleation sites are sensitive (Sha et al. 2013). In order to understand the notch sensitivity issue further, Singh and Narasimhan (2014) have recently conducted plane strain finite element simulations of tensile loading of rectangular specimens (48×96 nm) containing a circular edge notch with radius $R = 12$ nm and depth $D = 24$ nm using

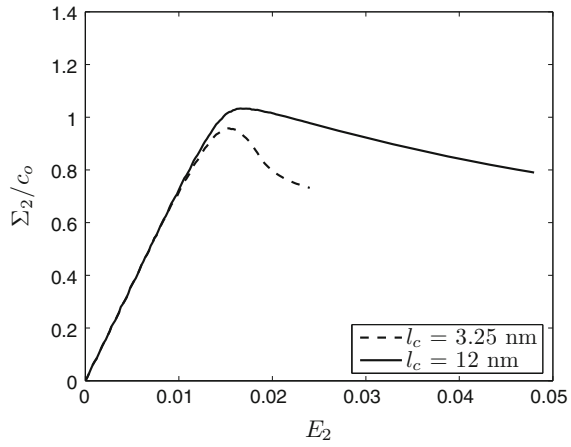

Fig. 18 Macroscopic stress Σ_2 normalized by initial cohesion c_o versus strain E_2 obtained from plane strain tension simulations of nanometer size notched MG samples by Singh and Narasimhan (2014). Results pertaining to two values of the internal material length scale l_c in the BMG constitutive model used in the simulations are shown

the BMG constitutive model of Thamburaja (2011). Two values of $l_c = 3.25$ and 12 nm were considered to investigate its effect on deformation behavior of MGs. Figure 18 shows the variation of the macroscopic stress Σ_2 (where X_1 is along the notch line and X_2 is parallel to the loading direction) normalized by initial cohesion c_o, with respect to global strain, E_2 for $l_c = 3.25$ and 12 nm. Rapid drop in stress suggesting shear localization after attainment of the peak can be seen at around $E_2 = 0.016$ for $l_c = 3.25$ nm. This is indeed confirmed from Fig. 19a which shows that the specimen will fail by unstable growth of a dominant SB (see shear offset m-m). In contrast, for higher $l_c = 12$ nm, Fig. 18 indicates that the stress decreases gradually after reaching a peak value. On examining the plastic strain contours displayed in Fig. 19b for this case, it can be noted that strain has accumulated almost entirely over the uncracked ligament (although there are two weak shear bands) and the specimen shows necking. Thus, these continuum simulation results corroborate with the experiments of Guo et al. (2007) and Jang and Greer (2010) and in particular with the conclusion made in the former that the presence of the notch may promote necking. Singh and Narasimhan (2014) have also made several other key observations about hardening and the role of interaction stress between flow defects in promoting this brittle–ductile transition in notched nanoscale MG samples.

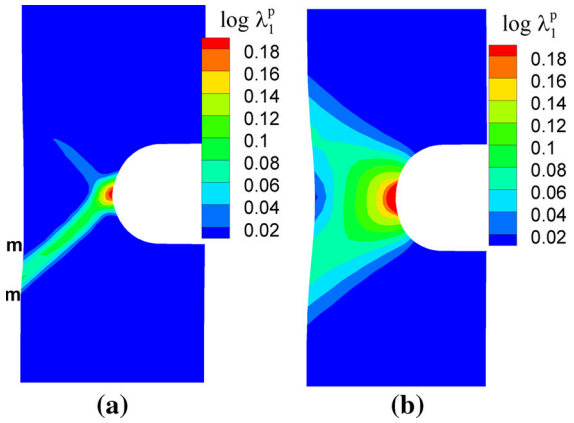

Fig. 19 Contour plots of $\log \lambda_1^p$ from plane strain tension simulations of nanometer size notched MG samples by Singh and Narasimhan (2014) corresponding to **a** $l_c = 3.25$ nm at 2 % strain and **b** $l_c = 12$ nm at 4.5 % strain

8 Toughness enhancement strategies

8.1 Compositional changes

The composition of BMGs can have a marked effect on the fracture resistance and mechanism of BMGs. Kim et al. (2009) noted that the addition of Ni and Fe to Zr-based BMGs can reduce the fracture toughness considerably. Lewandowski et al. (2008) systematically varied the chemical composition of Fe based BMGs so that ν is modified. They found that the fracture toughness increases from 5.7 to 46.7 MPa $m^{1/2}$ with increase in Poissions ratio from 0.314 to 0.33. There was also an increase in strain energy corresponding to shear failure in uniaxial compression tests of cylindrical specimens. The fracture surface of the alloy with high Poisson's ratio showed vein patterns characteristic of viscous flow. Jia et al. (2009) conducted experiments to measure the notched fracture toughness of Cu-based BMGs corresponding to different compositions. They found that the fracture toughness decreases with increasing Glass Forming Ability (GFA).

8.2 BMG composites

By introducing a second phase in a glassy matrix, propagating SBs and cracks can be arrested resulting in higher ductility and fracture toughness. Such materials are classified as BMG matrix composites (BMGCs) and fall under different sub-classes depending on the type of the second phase and the processing technique (Wang 2005; Trexler and Thadhani 2010). Following methods where reinforcements in the form of particulates were externally added (Choi-Yim and Johnson 1997; Choi-Yim et al. 1999; Eckert et al. 1999), Hays et al. (2000), and Szuecs et al. (2001) developed a process of precipitating an in situ ductile β phase (body centered cubic phase) within the BMG matrix. The alloy, called as LM2, developed by this process exhibited about 2.5 times the fracture toughness of the compositionally similar monolithic glass, Vit-1 which is attributed to the role of second phases in blocking/deflecting shear bands during fracture. Also, these second phases act as shear band initiation sites resulting in a large process zone.

Further developments in processing techniques by Hofmann et al. (2008a, b) resulted in BMGCs that possess a value of fracture toughness of around 157 MPa $m^{1/2}$ (Launey et al. 2009), which rivals the toughness of most crystalline materials. Zachrisson et al. (2011) observed that, higher toughness can be obtained when the microstructural length scales such as the inter-dendrite spacing and dendrite size are optimized with respect to the plastic zone size. In this context, introducing particulate inter-connectivity and using higher volume fractions are also expected to be beneficial (Fu et al. 2007). It must be noted that a ductile second phase gives better mechanical response than brittle crystallites embedded in the BMG matrix. Also a higher K_{Ic} of the BMG matrix adds to the propensity of shear banding in the composite (Chu et al. 2014).

8.3 Nanoglasses

Nanoglass (NG) was synthesized for the first time by Jing et al. (1989) via inert gas condensation followed by sintering of nanometer-sized amorphous spheres at high pressure. This gives rise to an architecture comprising of nanometer size glassy grains separated by fine interfaces. In recent studies, NGs have been synthesized using cold compaction and magnetron sputtering (Fang et al. 2012; Chen et al. 2013b). Experimental studies and atomistic simulations have shown that the interfaces are characterized by excess free volume or low density (Jing et al. 1989; Fang et al. 2012; Sopu et al. 2009; Ritter et al. 2011) and higher concentration of flow defects (STZs). Atomistic simulations have

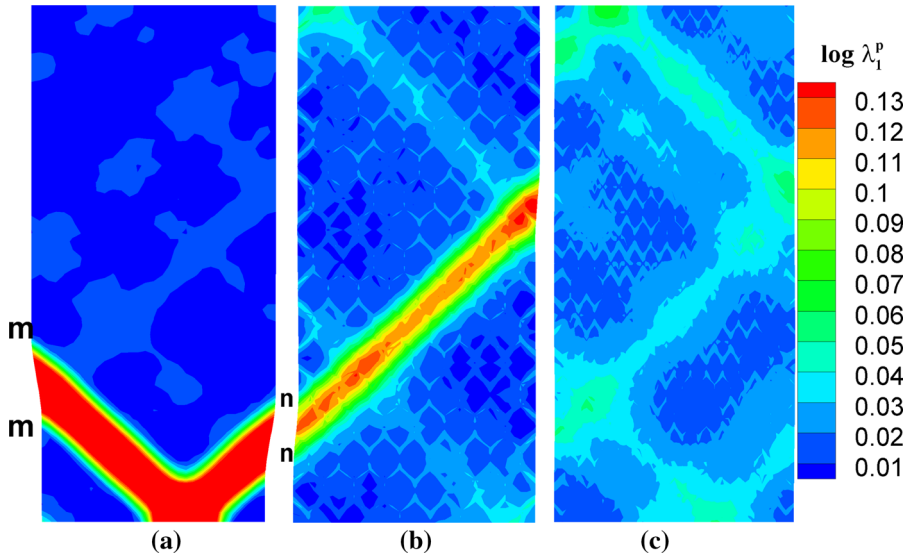

Fig. 20 Contour plots of maximum principal logarithmic plastic strain at macroscopic strain of 0.04 for **a** MG, **b** NG1 and **c** NG2 with $l_c = 3.25$ nm

also demonstrated that multiple SBs nucleate from soft interfaces leading to enhanced global plasticity (Albe et al. 2013; Sopu et al. 2011; Adibi et al. 2013, 2014). Also, the newly nucleated SBs do not cut through the grains at lower strain, whereas at larger strain they propagate through grains forming a dominant SB. Consequently, the ductility of NGs increases with decrease in grain size which may eventually lead to superplastic flow for average grain size below a threshold (Adibi et al. 2013). Recent atomistic simulations of NG samples with pre-existing notches have revealed that they fail through shear banding emanating from notch root due to high stress concentration when notch size is larger than the average grain size, whereas they exhibit notch insensitivity for smaller notch size (Sha et al. 2014).

In a recent work, Singh et al. (2014b) conducted 2D plane strain tension simulations of NGs using the nonlocal BMG constitutive model of Thamburaja (2011) in order to understand the physical origins of the length scale associated with above noted ductility enhancement. Singh et al. (2014b) assumed the NG architecture to be comprised of hexagonal grains (Albe et al. 2013) separated by 1 nm wide weak interfaces (Fang et al. 2012; Jing et al. 1989) with initial cohesion 20 % lower than the grain interior. Also, the cohesion in the interfaces was randomly perturbed by 1 % to trigger SBs. Two NGs with a large and small grain size, referred to as NG1 and NG2, respectively, were modeled, in addition to a BMG with no interfaces. The value of l_c in the BMG model (Thamburaja 2011) was varied to ascertain the effect of grain size relative to l_c on the deformation response.

Figure 20a–c present contour plots of $\log(\lambda_1^p)$ for the BMG, NG1 and NG2 corresponding to macroscopic strain of 0.04. It may be seen that plastic strain has localized in shear bands in the BMG and NG1 samples (Fig. 20a, b) leading to a strong shear offset marked as 'm–m' and 'n–n'. By contrast, NG2 continues to deform homogenously (Fig. 20c). Singh et al. (2014b) noted that the interaction stress between flow defects (STZs) plays a central role in delaying strain localization and this effect becomes stronger with reduction in grain size. Further, they showed that by reducing the ratio of grain size to the length scale l_c associated with the interaction stress, the tensile deformation behavior changes from shear banding to diffuse necking. Also they noted that moderate change in specimen size has no effect on the mechanical response of NGs unlike MGs (Thamburaja 2011).

9 Closing remarks

The present review has summarized the current understanding of mechanics and mechanisms of fracture in BMGs and methods being pursued for improving the fracture resistance and ductility of BMGs. Although there has been considerable volume of research on fracture of MGs, much work remains to be done. Some of

the outstanding issues in this connection that need to be resolved before MGs can be deployed into service where high reliability is required are listed below.

- As demonstrated by Tandaiya et al. (2013), the fracture process in a ductile BMG occurs within a dominant SB. Careful numerical simulations (possibly using multi-scale formulations) are needed to understand the failure processes that occur inside SBs, in which the material's response is like a liquid. As highlighted by Suh et al. (2010), 3D nature of shear banding needs to be studied through finite element simulations to gain an understanding of SB patterns and shear offsets within the bands.
- Contrasting trends on the variation of fracture toughness with mode mixity have been reported by Tandaiya et al. (2009) and Varadarajan et al. (2010). Thus, more experiments and complementary numerical simulations are needed to gain a clear understanding of mixed-mode fracture behavior for BMGs pertaining to different structural states and whether brittle–ductile transitions are possible with addition of mode II component of loading as predicted by Tandaiya et al. (2009). Likewise, more detailed studies on the effect of experimental variables such as strain rate and temperature on the fracture toughness are essential.
- In the context of brittle MGs, the mechanism of dynamic crack growth that results in the ubiquitous NCs, their origin and high periodicity requires further investigations. None of the existing models appear to satisfactorily explain the observed behaviors and there are gaps in understanding between atomistic, continuum simulations and experiments that need to be bridged. Cavitation studies need to be refined by employing appropriate BMG constitutive models that account for structural evolution (e.g., by Thamburaja 2011) and need to be coupled with crack tip fields, although some work in this direction has been performed by Henann and Anand (2009) and Rycroft and Bouchbinder (2012).
- Systematic experiments and simulations are needed to shed further light on issues such as notch sensitivity, toughness and ductility of BMGCs, NGs and nanoscale MG samples. The fundamental mechanism of plastic deformation such as STZ itself is not well understood in the context of dynamic cavitation, NGs and nanoscale components. Physics based theories backed by atomistic simulations are needed in this regard.
- It is now well established that MGs exhibit a sharp brittle-to-ductile transition (BDT) with temperature (Rabinovitch et al. 2006). Further, this BDT temperature is sensitive to the free volume content in the glass. 'What are the mechanistic reasons for BMGs exhibiting a BDT?' is a question that has not been answered comprehensively and detailed fracture experiments are needed to address this issue.
- Typically, the failure of components during service is triggered by crack initiation and growth under fatigue loading conditions. While it is now well established that BMGs are susceptible to fatigue just like their crystalline counterparts, precisely what leads to crack nucleation under cyclic loading conditions is not known. Likewise, there is a need to identify the mechanisms responsible for fatigue crack growth.

With improvement in their ductility and toughness through above suggested research and given their high strength, elastic strain and other attractive properties, MGs may become alternatives to crystalline metals in critical engineering applications.

Acknowledgments R.N. and U.R. would like to gratefully acknowledge the Department of Science and Technology (Government of India) for financial support under the JC Bose Fellowship scheme.

References

Adibi S, Sha ZD, Branicio PS, Joshi SP, Liu ZS, Zhang YW (2013) A transition from localized shear banding to homogeneous superplastic flow in nanoglass. Appl Phys lett 103:211905

Adibi S, Branicio PS, Zhang YW, Joshi SP (2014) Composition and grain size effects on the structural and mechanical properties of cuzr nanoglasses. J Appl Phys 116:043522

Albe K, Ritter Y, Sopu D (2013) Enhancing the plasticity of metallic glasses: shear band formation, nanocomposites and nanoglasses investigated by molecular dynamics simulations. Mech Mater 67:94–103

Anand L, Su C (2005) A theory for amorphous viscoplastic materials undergoing finite deformations, with application to metallic glasses. J Mech Phys Solids 53:1362–1396

Argon AS (1979) Plastic deformation in metallic glasses. Acta Metall 27:47–58

Argon AS, Salama M (1976) The mechanism of fracture in glassy materials capable of some inelastic deformation. Mater Sci Eng 23:219–230

Bhowmick R, Raghavan R, Chattopadhyay K, Ramamurty U (2006) Plastic flow softening in a bulk metallic glass. Acta Mater 54:4221–4228

Chen DZ, Jang D, Guan KM, An Q, Goddard WA, Greer JR (2013a) Nanometallic glasses: size reduction brings ductility, surface state drives its extent. Nano Lett 13:4462–4468

Chen N, Louzguine-Luzgin DV, Xie GQ, Inoue A (2009) Nanoscale wavy fracture surface of a Pd-based bulk metallic glass. Appl Phys Lett 94:131906

Chen N, Louzguine-Luzgin DV, Xie GQ, Sharma P, Perepezko JH, Esashi M, Yavari AR, Inoue A (2013b) Structural investigation and mechanical properties of a representative of a new class of materials: nanograined metallic glasses. Nanotechnol 24:045610

Choi-Yim H, Johnson WL (1997) Bulk metallic glass matrix composites. Appl Phys Lett 71:3808–3810

Choi-Yim H, Busch R, Köster U, Johnson W (1999) Synthesis and characterization of particulate reinforced $Zr_{57}Nb_5Al_{10}Cu_{15.4}Ni_{12.6}$ bulk metallic glass composites. Acta Mater 47:2455–2462

Chu Z, Yuan G, Kato H et al (2014) The effect of matrix fracture toughness on the plastic deformation of the metallic glassy composite. J Alloys Compd 612:10–15

Conner RD, Rosakis AJ, Johnson WL, Owen DM (1997) Fracture toughness determination for a beryllium-bearing bulk metallic glass. Scr Mater 37:1373–1378

De Hey P, Sietsma J, van den Beukel A (1998) Structural disordering in amorphous $Pd_{40}Ni_{40}P_{20}$ induced by high temperature deformation. Acta Mater 46:5873–5882

Donovan P (1989) A yield criterion for pd40ni40p20 metallic glass. Acta Metall 37:445–456

Duine PA, Sietsma J, van den Beukel A (1992) Defect production and annihilation near equilibrium in amorphous $Pd_{40}Ni_{40}P_{20}$ investigated from viscosity data. Acta Metal Mater 40:743–751

Eckert J, Schlorke-de Boer N (1999) Mechanically alloyed Mg-based metallic glasses and metallic glass composites containing nanocrystalline particles. Zeitschrift für Metallkunde 90:908–913

Falk ML (1999) Molecular-dynamics study of ductile and brittle fracture in model noncrystalline solids. Phys Rev B 60:7062–7070

Fang JX, Vainio U, Puff W, Wurschum R, Wang XL, Wang D, Ghafari M, Jiang F, Sun J, Hahn H, Gleiter H (2012) Atomic structure and structural stability of $Sc_{75}Fe_{25}$ nanoglasses. Nano Lett 12:458–463

Flores KM, Dauskardt RH (1999) Enhanced toughness due to stable crack tip damage zones in bulk metallic glass. Scr Mater 41:937–943

Flores KM, Dauskardt RH (2006) Mode II fracture behavior of a Zr-based bulk metallic glass. J Mech Phys Solids 54:2418–2435

Fu XL, Li Y, Schuh CA (2007) Temperature, strain rate and reinforcement volume fraction dependence of plastic deformation in metallic glass matrix composites. Acta Mater 55:3059–3071

Gao H (1993) Surface roughening and branching instabilities in dynamic fracture. J Mech Phys Solids 41:457–486

Gilbert CJ, Ritchie RO, Johnson WL (1997) Fracture toughness and fatigue-crack propagation in a ZrTiNiCuBe bulk metallic glass. Appl Phys Lett 71:476–478

Greer AL, Ma E (2007) Bulk metallic glasses: at the cutting edge of metals research. MRS Bull 32:611–619

Gu XJ, Poon SJ, Shiflet GJ, Lewandowski JJ (2009) Ductile-to-brittle transition in a Ti-based bulk metallic glass. Scr Mater 60:1027–1030

Guin JP, Widerhorn SM (2004) Fracture of silicate glasses : ductile or brittle. Phys Rev Lett 92:215502

Guo H, Yan PF, Wang YB, Tan J, Zhang ZF, Sui ML, Ma E (2007) Tensile ductility and necking of metallic glass. Nat Mater 6:735–739

Hasan HA, Kecskes L, Lewandowski J (2008) Effects of changes in test temperature and loading conditions on fracture toughness of a Zr-based bulk metallic glass. Metall Mater Trans A 39A:2077–2085

Hays CC, Kim CP, Johnson WL (2000) Microstructure controlled shear band pattern formation and enhanced plasticity of bulk metallic glasses containing in situ formed ductile phase dendrite dispersions. Phys Rev Lett 84:2901

Henann LD, Anand L (2009) Fracture of metallic glasses at notches: effects of notch-root radius and the ratio of the elastic shear modulus to the bulk modulus on toughness. Acta Mater 57:6057–6074

Hofmann DC, Suh J-Y, Wiest A et al (2008a) Designing metallic glass matrix composites with high toughness and tensile ductility. Nature 451:1085–1089

Hofmann DC, Suh J-Y, Wiest A, Johnson W (2008b) New processing possibilities for highly toughened metallic glass matrix composites with tensile ductility. Scr Mater 59:684–687

Horgan CO, Abeyaratne R (1986) A bifurcation problem for a compressible nonlinearly elastic medium: growth of a micro-void. J Elast 16:189–200

Horgan CO, Pence TJ (1989) Void nucleation in tensile deadloading of a composite incompressible nonlinearly elastic sphere. J Elast 21:61–82

Hou HS, Abeyaratne R (1992) Cavitation in elastic and elastic–plastic solids. J Mech Phys Solids 40:571–592

Huang Y, Hutchinson JW, Tvergaard V (1991) Cavitation instabilities in elasticplastic solids. J Mech Phys Solids 39:223–241

Hull D (1996) Influence of stress intensity and crack speed on fracture surface topography: mirror to mist to macroscopic bifurcation. J Mater Sci 31:1829–1841

Hull D (1995) The effect of mixed mode I/III on crack evolution in brittle solids. Int J Fract 70:59–79

Hull D (1999) Fractography: observing, measuring and interpreting fracture surface topography. Cambridge University Press, Cambridge

Jang D, Greer JR (2010) Transition from a strong-yet-brittle to a stronger-and-ductile state by size reduction of metallic glasses. Nat Mater 9:215–219

Jia P, Zd Zhu (2009) Notch toughness of cu-based bulk metallic glasses. Scr Mater 61:137–140

Jiang MQ, Ling Z, Meng JX et al (2010) Nanoscale periodic corrugation to dimple transition due to "beat" in a bulk metallic glass. Scr Mater 62:572–575

Jiang MQ, Ling Z, Meng JX, Dai LH (2008) Energy dissipation in fracture of bulk metallic glasses via inherent competition between local softening and quasi-cleavage. Philos Mag 88:407–426

Jiang MQ, Meng JX, Keryvin V, Dai LH (2011) Crack branching instability and directional stability in dynamic fracture of a tough bulk metallic glass. Intermetallics 19:1775–1779

Jing J, Kramer A, Birringer R, Gleiter H, Gonser U (1989) Modified atomic structure in a Pd–Fe–Si nanoglass: a Mössbauer study. J Non-Cryst Solids 113:167–170

Johnson WL, Samwer K (2005) A universal criterion for plastic yielding of metallic glasses with a $(T/T_g)^{2/3}$ temperature dependence. Phys Rev Lett 95:195501

Kai-feng Z, Li X, L X, Xi-feng LI (2007) New fracture morphology of amorphous Fe_{78} Si_9 B_{13} alloy. Trans Nonferrous Met Soc China 1:383–387

Kawashima A, Kurishita H, Kimura H et al (2005) Fracture Toughness of Zr∼5∼5Al∼1∼0Ni∼5Cu∼3∼ 0 bulk metallic glass by 3-point bend testing. Mater Trans 46:1725

Keryvin V, Bernard C, Sanglebœuf J-C et al (2006) Toughness of $Zr_{55}Cu_{30}Al_{10}Ni_5$ bulk metallic glass for two oxygen levels. J Non Cryst Solids 352:2863–2868

Kim CP, Suh JY, Wiest A, Johnson WL (2009) Fracture toughness study of new Zr-based Be-bearing bulk metallic glasses. Scr Mater 60:80–83

Klement W, Willens RH, Duwez P (1960) Non-crystalline structure in solidified gold–silicon alloys. Nature 187:869–870

Kumar G, Rector D, Conner RD, Schroers J (2009) Embrittlement of Zr-based bulk metallic glasses. Acta Mater 57:3572–3583

Langer JS (2008) Shear-transformation-zone theory of plastic deformation near the glass transition. Phys Rev E 77:021502

Launey ME, Hofmann DC, Suh J-Y et al (2009) Fracture toughness and crack-resistance curve behavior in metallic glass-matrix composites. Appl Phys Lett 94:241910

Leamy HJ, Wang TT, Chen HS (1972) Plastic flow and fracture of metallic glass. Metall Trans 3:699–708

Lewandowski JJ, Gu XJ, Shamimi NA, Poon SJ, Shiflet GJ (2008) Tough Fe-based bulk metallic glasses. Appl Phys Lett 92:09198

Lewandowski JJ, Shazly M, Nouri AS (2006) Intrinsic and extrinsic toughening of metallic glasses. Scr Mater 54:337–341

Lewandowski JJ, Wang WH, Greer AL (2005) Intrinsic plasticity or brittleness of metallic glasses. Philos Mag Lett 85:77–87

Li HX, Kim KB, Yi S (2007) Enhanced glass-forming ability of Fe-based bulk metallic glasses prepared using hot metal and commercial raw materials through the optimization of Mo content. Scr Mater 56:1035–1038

Lowhaphandu P, Lewandowski JJ (1998) Fracture toughness and notched toughness of bulk amorphous alloy: Zr-Ti-Ni-Cu-Be. Scr Mater 38:1811–1817

Lu J, Ravichandran G (2003) Pressure-dependent flow behavior of $Zr_{41.2}Ti_{13.8}Cu_{12.5}Ni_{10}Be_{22.5}$ bulk metallic glass. J Mater Res 18:2039–2049

Lund AC, Schuh CA (2003) Yield surface of a simulated metallic glass. Acta Mater 51:5399–5411

Ma RD, Zhang HF, Yu HS, Hu ZQ (2008) The effect of Al substitution on thermal and mechanical properties of Fe-based bulk metallic glass. J Alloys Compd 454:370–373

Madge SV, Wada T, Louzguine-Luzgin DV, et al (2009) Oxygen embrittlement in a Cu–Hf–Al bulk metallic glass. Scr Mater 61:540–543

Magagnosc DJ, Ehrbar R, Kumar G, He MR, Schroers J, Gianola DS (2013) Tunable tensile ductility in metallic glasses. Sci Rep 3:1096

McMeeking RM (1977) Finite deformation analysis of crack-tip opening in elastic–plastic materials and implications for fracture. J Mech Phys Solids 25:357–381

Murali P, Guo TF, Zhang YW, Narasimhan R, Li Y, Gao HJ (2011) Atomic scale fluctuations govern brittle fracture and cavitation behavior in metallic glasses. Phys Rev Lett 107:215501

Murali P, Ramamurty U (2005) Embrittlement of a bulk metallic glass due to sub-Tg annealing. Acta Mater 53:1467–1478

Nagendra N, Ramamurty U, Goh T, Li Y (2000) Effect of crystallinity on the impact toughness of a La-based bulk metallic glass. Acta Mater 48:2603–2615

Narasimhan R, Rosakis AJ (1990) Three-dimensional effects near a crack tip in a ductile three-point bend specimen: Part I—a numerical investigation. J Appl Mech 57: 607–617

Narayan RL, Tandaiya P, Narasimhan R, Ramamurty U (2014) Wallner lines, crack velocity and mechanisms of crack nucleation and growth in a brittle bulk metallic glass. Acta Mater 80:407–420

Packard CE, Franke O, Homer ER, Schuh CA (2010) Nanoscale strength distribution in amorphous versus crystalline metals. J Mater Res 25:2251–2263

Pampillo CA (1975) Flow and fracture in amorphous alloys. J Mater Sci 10:1194–1227

Pan DG, Zhang HF, Wang AM et al (2007) Fracture instability in brittle Mg-based bulk metallic glasses. J Alloys Compd 438:145–149

Patnaik MNM, Narasimhan R, Ramamurty U (2004) Spherical indentation response of metallic glasses. Acta Mater 52:3335–3345

Pugh SF (1954) Relations between the elastic moduli and the plastic properties of polycrystalline pure metals. Philos Mag 45:823–843

Qu RT, Stoica M, Eckert J, Zhang ZF (2010) Tensile fracture morphologies of bulk metallic glass. J Appl Phys 108:063509

Rabinovitch A, Frid V, Bahat D (2006) Wallner lines revisited. J Appl Phys 99:076102

Raghavan R, Murali P, Ramamurty U (2006) Ductile to brittle transition in the $Zr_{41.2}Ti_{13.75}Cu_{12.5}Ni_{10}Be_{22.5}$ bulk metallic glass. Intermetallics 14:1051–1054

Ravi-Chandar K (2004) Dynamic fracture. Elsevier, Amsterdam

Ravi-Chandar K, Yang B (1997) On the role of microcracks in the dynamic fracture of brittle materials. J Mech Phys Solids 45:535–563

Rice JR, Johnson MA (1970) The role of large crack tip geometry changes in plane strain fracture. In: Kanninen ME, Adler WE, Rosenfield AR, Jaffee RI (eds) Inelastic behavior of solids. McGraw-Hill, New York, pp 641–672

Rice JR, Levy N (1969) Local heating by plastic deformation at a crack tip. In: Argon AS (ed) Physics of strength and plasticity. MIT Press, Cambridge. pp 277–293

Rice JR, Thomson R (1974) Ductile versus brittle behaviour of crystals. Philos Mag 29:73–97

Ritter Y, Sopu D, Gleiter H, Albe K (2011) Structure, stability and mechanical properties of internal interfaces in $Cu_{64}Zr_{36}$ nanoglasses studied by MD simulations. Acta Mater 59:6588–6593

Rycroft CH, Bouchbinder E (2012) Fracture toughness of metallic glasses: annealing-induced embrittlement. Phys Rev Lett 109:194301

Saffman PG, Taylor G (1958) The penetration of a fluid into a porous medium or Hele–Shaw cell containing a more viscous liquid. Proc R Soc Lond A 245:312–329

Schroers J, Johnson WL (2004) Ductile bulk metallic glass. Phys Rev Lett 93:255506

Schuh CA, Hufnagel TC, Ramamurty U (2007) Mechanical behavior of amorphous alloys. Acta Mater 55:4067–4109

Sha ZD, Pei QX, Sorkin V, Branicio PS, Zhang YW, Gao H (2013) On the notch sensitivity of cuzr metallic glasses. Appl Phys Lett 103:081903

Sharon E, Cohen G, Fineberg J (2002) Crack front waves and the dynamics of a rapidly moving crack. Phys Rev Lett 88:085503

Sha ZD, He LC, Pei QX, Pan H, Liu ZS, Zhang YW, Wang TJ (2014) On the notch sensitivity of CuZr nanoglass. J Appl Phys 115:163507

Shen J, Liang WZ, Sun JF (2006) Formation of nanowaves in compressive fracture of a less-brittle bulk metallic glass. Appl Phys Lett 89:121908. doi:10.1063/1.2356083

Singh I, Guo TF, Murali P, Narasimhan R, Zhang YW, Gao HJ (2013) Cavitation in materials with distributed weak zones: implications on the origin of brittle fracture in metallic glasses. J Mech Phys Solids 61:1047–1064

Singh I, Guo TF, Narasimhan R, Zhang YW (2014a) Cavitation in brittle metallic glasses—effects of stress state and distributed weak zones. Int J Solids and Struct. doi:10.1016/j.ijsolstr.2014.09.005

Singh I, Narasimhan R (2014) Notch sensitivity in nanoscale metallic glass specimens: insights from continuum simulations, manuscript under preparation for publication

Singh I, Narasimhan R, Zhang YW (2014b) Ductility enhancement in nanoglass: role of interaction stress between flow defects. Philos Mag Lett 94:1–10

Sommer E (1969) Formation of fracture "lances" in glass. Eng Fract Mech 1:539–546

Sopu D, Albe K, Ritter Y, Gleiter H (2009) From nanoglasses to bulkmassive glasses. Appl Phys Lett 94:191911

Sopu D, Ritter Y, Gleiter H, Albe K (2011) Deformation behavior of bulk and nanostructured metallic glasses studied via molecular dynamics simulations. Phys Rev B Condens Matter Mater Phys 83:100202

Spaepen F (1977) A microscopic mechanism for steady state inhomogeneous flow in metallic glasses. Acta Metall 25:407–415

Suh J, Conner R, Kim C, Demetriou M, Johnson W (2010) Correlation between fracture surface morphology and toughness in Zr-based bulk metallic glasses. J Mater Res 25:982–990

Szuecs F, Kim CPP, Johnson WLL, SZUECST F (2001) Mechanical properties of $Zr_{56.2}Ti_{13.8}Nb_{5.0}Cu_{6.9}Ni_{5.6}Be_{12.5}$ ductile phase reinforced bulk metallic glass composite. Acta Mater 49:1507–1513

Tan J, Zhang Y, Sun BA et al (2011) Correlation between internal states and plasticity in bulk metallic glass. Appl Phys Lett 98:151906

Tandaiya P, Narasimhan R, Ramamurty U (2007) Mode I crack tip fields in amorphous materials with application to metallic glasses. Acta Mater 55:6541–6552

Tandaiya P, Ramamurty U, Ravichandran G, Narasimhan R (2008) Effect of Poisson's ratio on crack tip fields and fracture behavior of metallic glasses. Acta Mater 56:6077–6086

Tandaiya P, Ramamurty U, Narasimhan R (2009) Mixed mode (I and II) crack tip fields in bulk metallic glasses. J Mech Phys Solids 57:1880–1897

Tandaiya P, Narasimhan R, Ramamurty U (2013) On the mechanism and the length scales involved in the ductile fracture of a bulk metallic glass. Acta Mater 61:1558–1570

Thamburaja P (2011) Length scale effects on the shear localization process in metallic glasses: a theoretical and computational study. J Mech Phys Solids 59:1552–1575

Tian L, Cheng YQ, Shan ZW, Li J, Wang CC, Han XD, Sun J, Ma E (2012) Approaching the ideal elastic limit of metallic glasses. Nat Commun 3:609

Trexler MM, Thadhani NN (2010) Mechanical properties of bulk metallic glasses. Prog Mater Sci 55:759–839

Varadarajan R, Thurston A, Lewandowski J (2010) Increased toughness of zirconium-based bulk metallic glasses tested under mixed mode conditions. Metall Mater Trans A 41A:149–158

Varias AG, Suo Z, Shih CF (1991) Ductile failure of a constrained metal foil. J Mech Phys Solids 39:963–986

Wang G, Chan KC, Xu XH, Wang WH (2008) Instability of crack propagation in brittle bulk metallic glass. Acta Mater 56:5845–5860

Wang G, Wang YT, Liu YH et al (2006) Evolution of nanoscale morphology on fracture surface of brittle metallic glass. Appl Phys Lett 89:121909

Wang G, Zhao DQ, Bai HY et al (2007) Nanoscale periodic morphologies on the fracture surface of brittle metallic glasses. Phys Rev Lett 98:235501

Wang H (2005) Bulk metallic glass composites. J Mater Sci Technol 21:86–90

Wang YT, Xi XK, Wang G et al (2009) Understanding of nanoscale periodic stripes on fracture surface of metallic glasses. J Appl Phys 106:113528

Xi XK, Zhao DQ, Pan MX et al (2005) Fracture of brittle metallic glasses: brittleness or plasticity. Phys Rev Lett 94:125510

Xi XK, Zhao DQ, Pan MX et al (2006) Periodic corrugation on dynamic fracture surface in brittle bulk metallic glass. Appl Phys Lett 89:18191

Xia XX, Wang WH (2012) Characterization and modeling of breaking-induced spontaneous nanoscale periodic stripes in metallic glasses. Small 8:1197–1203

Xu J, Ramamurty U, Ma E (2010) The fracture toughness of bulk metallic glasses. JOM 62(4):10–18

Yajuan S, Xianshun W, Yongjiang H, Jun S (2009) Effect of Gd addition on the glass forming ability and mechanical propertiese in a Zr- based bulk amorphous alloy. Acta Metall Sin 45:243–248

Zachrisson C, Kozachkov H, Roberts S et al (2011) Effect of processing on Charpy impact toughness of metallic glass matrix composites. J Mater Res 26:1260–1268

Zhang ZFFZ, Wu FFF, Gao W et al (2006) Wavy cleavage fracture of bulk metallic glass. Appl Phys Lett 89:251917

Zhao JX, Qu RT, Wu FF et al (2009) Fracture mechanism of some brittle metallic glasses. J Appl Phys 105:103519

Zink M, Samwer K, Johnson WL, Mayr SG (2006) Plastic deformation of metallic glasses: size of shear transformation zones from molecular dynamics simulations. Phys Rev B 73:172203